

## Chapter 6

# Cardiac and Respiratory Motion of the Coronary Arteries

This chapter presents an analysis of the motion of the coronary arteries from free breathing coronary angiograms. Anatomic landmarks were systematically identified on the left and right coronary trees, which enabled the comparison of results across patients. Three dimensional displacements and velocities were measured independently for the cardiac cycle and the respiratory cycle. Quiescent rest periods of minimum coronary motion were quantified for the two motion fields.

The implications of these results for magnetic resonance coronary angiography is described. The presence of rest periods during the cardiac and respiratory cycles means that images free of motion artifacts can be acquired. The motion of the arteries during breathing was analyzed using three linear motion models that correspond to available MR motion correction techniques: translation, rigid body, and affine. We address the potential of each motion model for increasing scan efficiency and reducing total scan duration, while maintaining image quality.

---

Work from this chapter was presented at the International Society for Magnetic Resonance in Medicine 2004 Meeting [113].

## 6.1 Method

### 6.1.1 Imaging Protocol

Conventional cine biplane coronary angiograms were obtained in 8 male and 2 female patients referred for diagnostic left heart catheterization. All patients gave written informed consent to participate in this institutional review board approved study. Their mean age was  $65 \pm 11$  years (range, 51-85 years). Four patients had mild dilated cardiomyopathy, and two had mild to moderate hypertrophic disease. The mean ejection fraction as measured by ventriculography was  $58 \pm 8\%$  (range, 40-65%).

All images were acquired on a Siemens biplane HICOR Angiography unit (Siemens, Erlangen, Germany). Images were acquired at 30 frames per second, digitized, and archived onto a CD in DICOM (Digital Imaging and Communications in Medicine) format. The raw 512x512 images were extracted using custom software on a personal computer running Linux, and all post processing was performed using MATLAB (The MathWorks Inc., Natick, MA, USA).

Each patient's ECG was recorded using a separate digital acquisition system, which also received timing signals from the Siemens imaging system. This setup enabled each image to be assigned a cardiac phase. Coronary arteriography was performed using conventional techniques. The bolus injection of iodinated contrast lasted 3 to 6 seconds, capturing several cardiac cycles and approximately one respiratory cycle of motion. We imaged spontaneous tidal respiration by not giving the patients any instruction related to their breathing.

For each configuration of the imaging system (primary and secondary angles, source-intensifier distance) used in the acquisition of coronary images, we also acquired images of a dewarping and calibration phantom. The dewarping phantom was a thin sheet of plastic ( $23 \times 23 \times 0.2$  cm) containing 1 mm diameter stainless steel balls arranged in a Cartesian grid pattern with 1 cm vertical and horizontal spacing. It was imaged while affixed to the face of the image intensifier tube. The calibration phantom was a  $9.8 \times 12.1 \times 3.8$  cm plastic block containing 19 stainless steel beads in a known configuration. It was placed at the system iso-center and imaged in biplane.

## 6.1.2 Motion Reconstruction

### Reconstructing Coronary Artery Motion

A static 3D model of the coronary arteries was reconstructed for each dataset using methods described in Chapter 3. One biplane pair of images was selected at diastasis, to minimize the motion of and to maximize the separation of arteries in the projection images. The images were processed with filters that enhance the location of arteries [99], and the arterial centerlines were semi-automatically drawn in the two images. Point to point correspondences between the arteries drawn in the two projections were computed automatically [73] and a 3D reconstruction was generated using knowledge of the geometric configuration of the imaging system.

Using the static coronary tree model as an initial state, the 3D motion of the arteries was recovered using the automatic motion tracking algorithm described in Chapter 4 [79]. The algorithm computes the best 3D transformation of the coronary tree model, so that the projection of the arteries is consistent with the temporally changing image sequence.

### Separating Cardiac and Respiratory Motion

The motion field recovered for each coronary angiogram dataset captures the motion of the coronary arteries while the heart is beating and the patient is breathing. Each deformation step, which corresponds to a biplane image pair is assigned a cardiac and respiratory phase. The cardiac phase ( $\chi$ ) represents the percentage of the cardiac cycle with the QRS peak at  $\chi=0$ . Intra-patient and inter-patient heart rate variability is normalized by calculating the systolic and diastolic intervals for each heart beat using the method of [103]. For each beat, the systolic interval was linearly rescaled between  $[0, 0.42)$ , which corresponds to the systolic interval of a 60 beat per minute heart rate. The diastolic interval was rescaled between  $[0.42, 1)$ .

The respiratory phase ( $\rho$ ) is measured directly from the images by taking a profile through the diaphragm. The displacement of the diaphragm-lung interface relative to end-expiration is used as a measure of respiratory phase.  $\rho=0$  at end expiration, and  $\rho=\pm 1$  at end inspiration. The sign of  $\rho$  depends on whether the image is acquired

during inspiration (+) or expiration (-).

A parametric cardiac respiratory model is used to decompose the field into independent cardiac and respiratory motion components (see Chapter 5 for details). The parametric model is used to create two synthetic motion fields. The first represents a cardiac contraction in the absence of respiratory motion. The second contains a cycle of respiratory motion in the absence of cardiac motion.

### 6.1.3 Data Evaluation

The right coronary artery (RCA) was studied in four patients. The RCA was qualitatively divided into proximal, middle, and distal thirds by an interventional cardiologist (Figure 6.1) [114]. Three points along the RCA were selected for study:

1.  $RCA_O$ : the right coronary ostium;
2.  $RCA_{(.5)AM}$ : the point of intersection of the proximal and middle thirds, which is approximately one-half the distance from the ostium to the acute margin of the heart; and
3.  $RCA_{AM}$ : the point of intersection of the middle and distal thirds, which is the acute margin of the heart.

The mean 3D length of the reconstructed proximal third of the RCA was  $38.7 \pm 9.5$  mm (range, 29.0-43.0 mm). The mean 3D length of the middle third of the RCA was  $36.3 \pm 4.9$  mm (range, 31.5-42.5 mm). The left coronary tree was studied in seven patients. Four landmarks were systematically identified for further study:

1.  $LM_O$ : the left main (LM) origin;
2.  $LM_B$ : the point where the LM bifurcates into the left anterior descending (LAD) artery and the left circumflex artery (LCx);
3.  $LAD_5$ : a point on the LAD five centimeters away from the LM origin; and
4.  $LCx_5$ : a point on the LCx five centimeters away from the LM origin.

The mean 3D length of the LM was  $14.2 \pm 3.8$  mm (range, 8.4-19.0 mm).

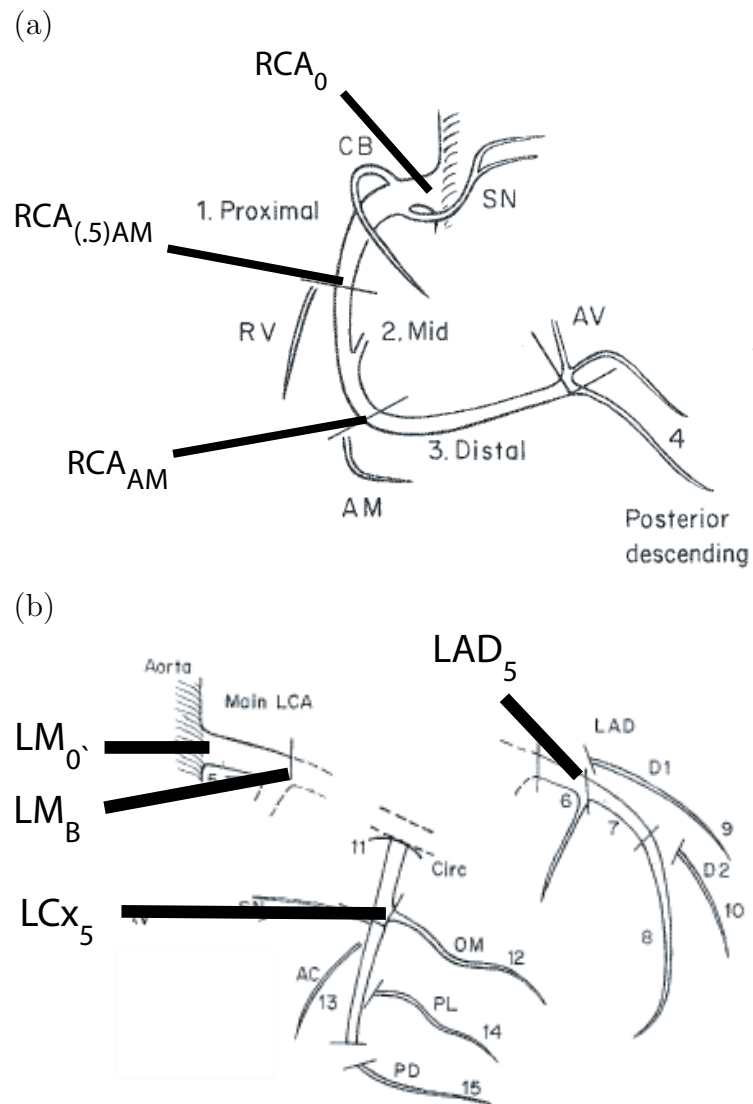


Figure 6.1: Landmarks on the right and left coronary artery trees were selected using the reporting system of Austen *et al.* [112]. (Figures borrowed from the original publication.)

## Displacement

Applying the motion field representing only the cardiac contraction to the 3D coronary tree models, we measured the 3D cardiac motion of the landmarks. The respiratory motion was frozen at end-expiration. The 1D cardiac displacements are reported with respect to the patient's left-right (LR), inferior-superior (IS), and posterior-anterior (PA) axes. The reference zero displacement was at the onset of ventricular systole ( $\chi=0$ ).

Using the respiration-only motion field, the same measurements were made to quantify the respiratory motion of the coronary arteries. The reference zero displacement was at end-expiration ( $\rho=0$ ). For the respiratory motion analysis, the cardiac motion field was frozen at mid-diastole.

## Velocity

The velocity of a point was computed by taking finite differences of its position. Since these velocities were calculated with respect to a normalized 60 beat per minute heart rate ( $dx/d\chi$ ), we multiplied by a patient specific correction factor ( $d\chi/dt$ ) to obtain true velocities ( $dx/dt$ ). The maximum velocity was determined for each patient during three three sub-phases of the cardiac cycle: (1) systole ( $0 \leq \chi < 0.42$ ); (2) the rapid filling phase of early diastole ( $0.42 \leq \chi < 0.70$ ); and (3) atrial contraction ( $0.80 \leq \chi < 1.00$ ). The maximum velocities are reported as a mean and standard deviation for the set of patients. In a similar fashion, minimum velocities were determined at end-systole ( $0.25 \leq \chi < 0.55$ ) and mid-diastole ( $0.6 \leq \chi < 0.9$ ).

Respiratory velocity was calculated in a similar manner. Since these velocities were calculated with respect to the respiratory phase ( $dx/d\rho$ ), we multiplied by the dwell time  $d\rho/dt$  of each respiratory phase to obtain the velocity with respect to time ( $dx/dt$ ). Minimum velocities were computed at end-inspiration ( $\rho=\pm 1$ ) and end-expiration ( $\rho=0$ ). Mean and peak velocities were calculated separately for expiration ( $-1 < \rho < 0$ ) and inspiration ( $0 < \rho < 1$ ).

## Rest Period

The cardiac and respiratory motion was analyzed to identify quiescent periods. The rest period was defined as the amount of time during which the motion of the coronary tree was within some upper bound. The upper bound can be thought of as the allowed 3D motion of points on the coronary tree.

To evaluate the rest period duration at different cardiac phases, we sampled the cardiac cycle at 100 cardiac phases  $\chi$ . With  $\chi_i$  as the reference location, the rest period was defined as the longest symmetric time window around  $\chi_i$ , such that the motion of all the points on the tree, during that time interval, is below the allowed 3D motion limit.

The respiratory rest period was analogously computed at 100 samples of  $\rho$ . Respiratory rest period durations were reported in milliseconds, and as a percentage of the patient's respiratory cycle in an attempt to normalize for the variability in breathing rate.

## Statistics

Measurements are reported as a mean $\pm$ one standard deviation. Displacements, velocities, and rest period durations were compared using a two-tailed Student's t-test with significance level of 0.05. The t-test for paired samples was used when appropriate. Multiple pairwise comparisons were performed using a Bonferroni t-test [115].

## 6.2 Results: Cardiac Motion

In the four right coronary datasets, the patients had a mean heart rate of  $64 \pm 9$  beats per minute (range, 55-75 beats per minute). In the seven left coronary datasets, the patients had a mean heart rate of  $64 \pm 7$  beats per minute (range, 56-74 beats per minute).

### 6.2.1 Displacement

#### Right Coronary

The displacement of the RCA ostium over the cardiac cycle in four patients is shown in Figure 6.2. The shape of the 3D displacement curve has several basic segments:

1. a large rapid systolic motion from  $\chi \approx 0$  to  $\chi \approx 0.4$
2. a variable length end-systolic period of stasis at  $\chi \approx 0.4$
3. a rapid motion corresponding to early diastolic filling from  $\chi \approx 0.4$  to  $\chi \approx 0.6$
4. a static period at mid-diastole (diastasis) from  $\chi \approx 0.6$  to  $\chi \approx 0.8$
5. a rapid motion corresponding to the atrial contraction from  $\chi \approx 0.8$  to  $\chi \approx 0.1$

Individual patient variability affects the shape and duration of these features.

The maximum 3D displacement of the RCA ostium ranged between 13.0-17.2 mm in four patients. The range of the maximal displacement of  $RCA_{(0.5)AM}$  and  $RCA_{AM}$  was 22.9-29.7 mm and 20.9-24.7 mm respectively.

The maximum 3D displacement of the RCA ostium during the cardiac cycle (mean,  $14.4 \pm 1.9$  mm) was significantly less than the peak 3D displacement of the distal landmarks,  $RCA_{(0.5)AM}$  (mean  $26.3 \pm 3.1$  mm,  $P < 0.001$ , Bonferroni t-test with three comparisons), and  $RCA_{AM}$  (mean  $23.2 \pm 1.6$  mm,  $P < 0.003$ , Bonferroni t-test with three comparisons).

A summary of the peak 1D and 3D displacements over the cardiac cycle, at three different points along the RCA, is presented in Table 6.1. As the heart contracted,

Table 6.1: Maximum displacement of the right coronary artery during the cardiac contraction (at end-expiration). The results are the mean and standard deviation for four patients. Positive displacements are toward the left, inferior, and posterior, respectively.

Right Coronary Landmark	Displacement: Cardiac Contraction			
	3D (mm)	LR (mm)	IS (mm)	AP (mm)
RCA <sub>O</sub>	14.4 ± 1.9	8.7 ± 1.7	4.6 ± 0.3	-11.0 ± 2.6
RCA <sub>(.5)AM</sub>	26.3 ± 3.1	15.0 ± 1.8	7.2 ± 1.6	-20.4 ± 4.0
RCA <sub>AM</sub>	23.2 ± 1.6	12.3 ± 2.6	6.2 ± 1.7	-18.3 ± 3.2

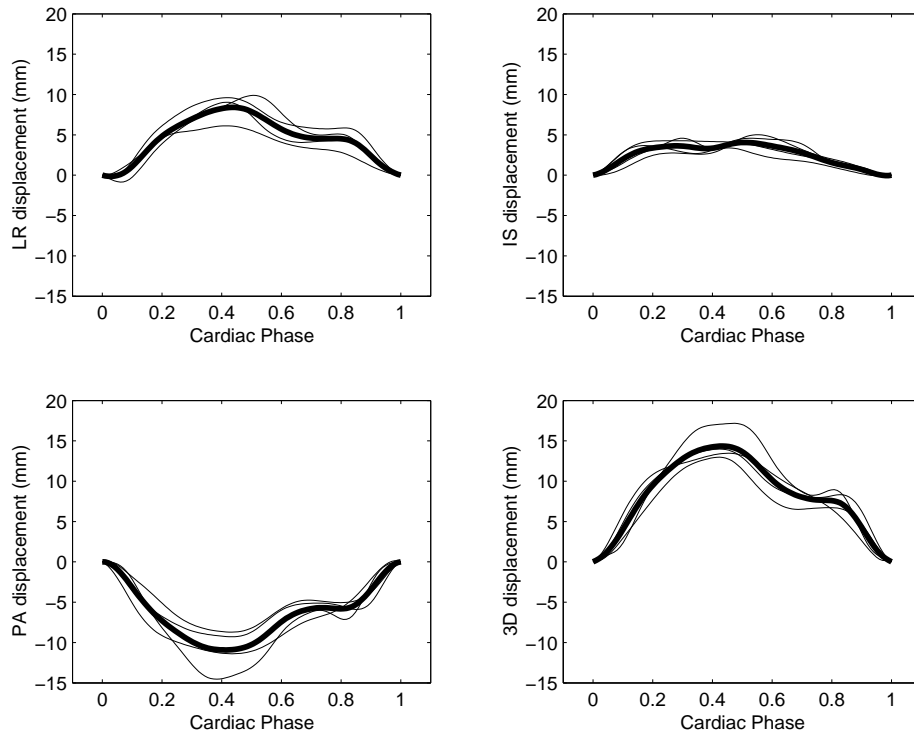


Figure 6.2: Displacement of the RCA origin during the cardiac contraction (at end-expiration). The plots show individual results for four patients (thin lines) and the mean displacement (thick line). The 1D displacements are with respect to the patient’s left-right (LR), inferior-superior (IS), and posterior-anterior (PA) axes. Positive displacements are toward the left, inferior, and posterior, respectively. The magnitude of the 3D displacement is shown in the bottom right plot.

the motion of the landmarks was consistently oriented toward the left, inferior, and anterior.

Most of the motion was directed along the anterior–posterior axis, and the least in the inferior-superior direction. For example, at the peak 3D displacement of the RCA ostium, the motion was  $46\pm 6\%$  in the AP axis,  $37\pm 7\%$  in the LR axis, and  $17\pm 2\%$  in the IS axis. Similarly, the breakdown was  $50\pm 10\%$ ,  $33\pm 6\%$ , and  $16\pm 5\%$  at  $\text{RCA}_{AM}$ .

### Left Coronary

The displacement of the LM ostium over the cardiac cycle in seven patients is shown in Figure 6.3. The shape of the curves is similar to these shown for the right coronary artery, but the left coronary curves have a smaller amplitude.

The range of the maximum 3D displacement of the left coronary landmarks was identified in the seven patients. The range was between 3.8-10.1 mm at the LM ostium, 5.6-10.6 mm at the LAD-LCx bifurcation, 8.5-12.1 mm at  $\text{LAD}_5$ , and 9.6-16.2 mm at  $\text{LCx}_5$ .

The peak 3D displacement of the left circumflex landmark during the cardiac cycle (mean,  $12.1\pm 2.4$  mm) was significantly higher than the peak 3D displacement of  $\text{LM}_0$  (mean,  $7.9\pm 2.2$  mm,  $P<0.001$ ),  $\text{LM}_B$  (mean,  $8.5\pm 1.7$  mm,  $P<0.001$ ), and  $\text{LAD}_5$  (mean,  $9.6\pm 1.3$  mm,  $P<0.004$ , Bonferroni t-test with six comparisons).

A summary of the peak 1D and 3D displacements over the cardiac cycle, at four different points on the left coronary tree, is presented in Table 6.2. As the heart contracted, the motion of the landmarks was consistently directed toward the left, inferior, and anterior. The motion was equally distributed over the three principle axes. For example, at the time of peak 3D displacement of the LM ostium, the motion was  $33\pm 11\%$  in the LR axis,  $31\pm 8\%$  in the IS axis, and  $36\pm 11\%$  in the PA axis.

Table 6.2: Maximum displacement of the left coronary tree during the cardiac contraction (at end-expiration). The results are the mean and standard deviation for seven patients. Positive displacements are toward the left, inferior, and posterior, respectively.

Left Coronary Landmark	Displacement: Cardiac Contraction			
	3D (mm)	LR (mm)	IS (mm)	AP (mm)
$LM_O$	$7.9 \pm 2.2$	$4.8 \pm 2.2$	$4.3 \pm 1.1$	$-4.6 \pm 1.6$
$LM_B$	$8.5 \pm 1.7$	$5.3 \pm 1.8$	$4.7 \pm 0.6$	$-4.9 \pm 1.5$
$LAD_5$	$9.6 \pm 1.3$	$5.0 \pm 2.3$	$5.7 \pm 0.9$	$-4.8 \pm 3.5$
$LCx_5$	$12.1 \pm 2.4$	$6.8 \pm 3.4$	$7.3 \pm 1.9$	$-6.8 \pm 1.8$

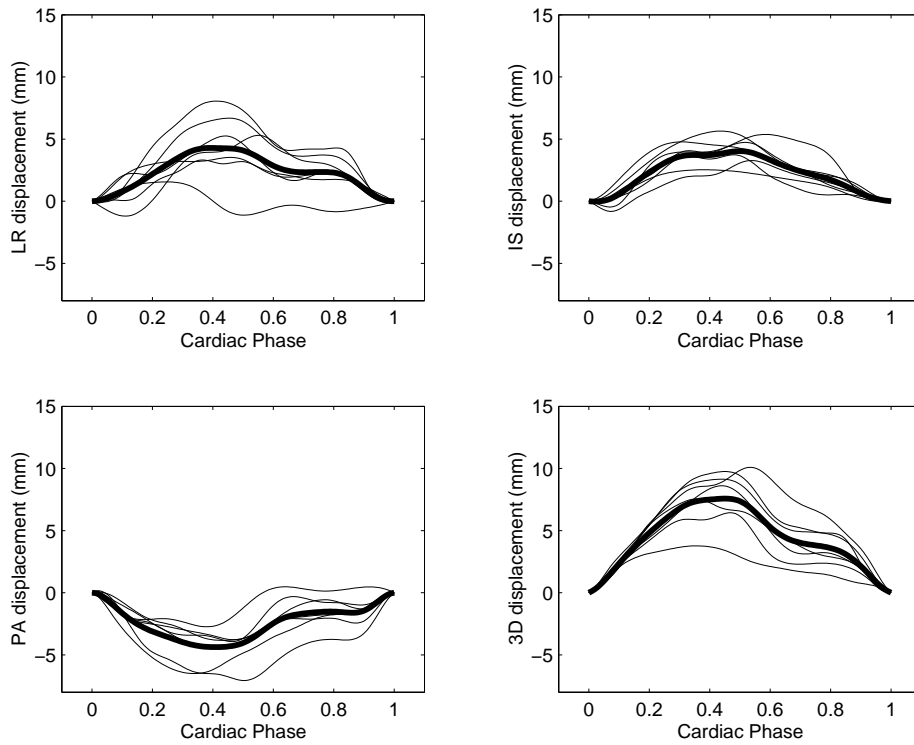


Figure 6.3: Displacement of the LM origin during the cardiac contraction (at end-expiration). The plots show individual results for four patients (thin lines) and the mean displacement (thick line). The 1D displacements are with respect to the patient’s left-right (LR), inferior-superior (IS), and posterior-anterior (PA) axes. Positive displacements are toward the left, inferior, and posterior, respectively. The magnitude of the 3D displacement is shown in the bottom right plot.

## 6.2.2 Velocity

### Right Coronary

The velocity of the RCA landmarks over the cardiac cycle is plotted in Figure 6.4. The velocity profile curve has several features:

1. a systolic peak corresponding to the cardiac contraction at  $0 < \chi < 0.2$
2. an end-systolic low velocity period at  $\chi \approx 0.4$
3. a peak corresponding to the rapid motion during early diastolic filling at  $\chi \approx 0.5$
4. a low-velocity period at mid-diastole (diastasis) at  $\chi \approx 0.75$
5. a high-velocity period corresponding to the atrial contraction at  $0.8 < \chi < 1$

Individual patient variability affects the shape, location, and duration of these features.

The peak values for the three high velocity phases of the cardiac cycle are summarized in Table 6.3 for four patients. The inter-patient range of peak velocity was 50.6-150.3 mm/s during systole, 19.7-120.0 mm/s during early diastole, and 33.0-174.2 mm/s during the atrial contraction.

Distal portions of the RCA were found to have higher velocities than proximal regions. During systole, the peak velocity at at  $RCA_{(0.5)AM}$  (mean,  $130.7 \pm 19.4$  mm/s) was statistically higher than the peak velocity at the RCA ostium (mean,  $69.8 \pm 13.8$  mm/s,  $P < 0.001$ , Bonferroni t-test with three comparisons).

The minimum velocities at end-systole and in diastasis are summarized in Table 6.4. The inter-patient range of minimum velocity was 2.2-14.7 mm/s at end-systole, and 5.1-21.4 mm/s during diastasis.

The minimum velocities during end-systole and in diastasis were significantly less than the peak velocities during systole, early-diastole, and atrial contraction, but were not statistically different from each other (Bonferroni t-test with 10 comparisons). At  $RCA_0$  the minimum end-systolic velocity was  $7.5 \pm 6.0$  mm/s, and the minimum velocity at diastasis was  $9.2 \pm 3.9$  mm/s.

Table 6.3: Maximum 3D velocity of the right coronary artery during the cardiac contraction in millimeters per second (mm/s). The results are the mean and standard deviation for four patients.

Right Coronary Landmark	Maximum Velocity: Cardiac Contraction		
	Systole (mm/s)	Diastolic Filling (mm/s)	Atrial Contraction (mm/s)
$RCA_O$	$69.8 \pm 13.8$	$41.1 \pm 15.0$	$63.0 \pm 21.4$
$RCA_{(0.5)AM}$	$130.7 \pm 19.4$	$70.4 \pm 36.2$	$120.8 \pm 46.7$
$RCA_{AM}$	$101.8 \pm 13.4$	$60.1 \pm 23.8$	$103.4 \pm 40.7$

Table 6.4: Minimum 3D velocity of the right coronary artery during the cardiac contraction in millimeters per second (mm/s). The results are the mean and standard deviation for four patients.

Right Coronary Landmark	Minimum Velocity: Cardiac Contraction	
	End-Systole (mm/s)	Diastasis (mm/s)
$RCA_O$	$7.5 \pm 6.0$	$9.2 \pm 3.9$
$RCA_{(0.5)AM}$	$10.4 \pm 5.1$	$12.8 \pm 6.3$
$RCA_{AM}$	$7.3 \pm 3.4$	$13.1 \pm 5.8$

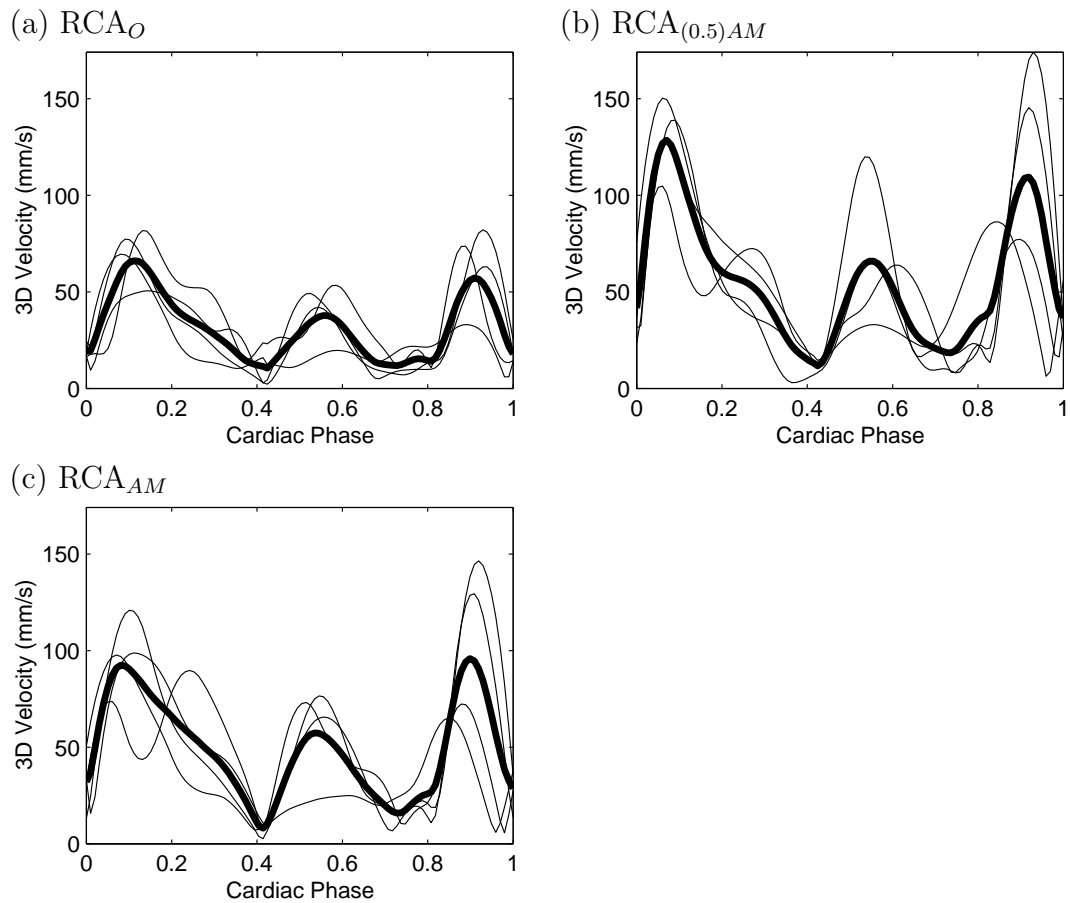


Figure 6.4: Velocity of the right coronary artery during the cardiac contraction (at end-expiration). The plot shows individual results for four patients (thin lines) and the mean velocity (thick line).  $RCA_O$ : the RCA origin.  $RCA_{(0.5)AM}$ : a point approximately one-half the distance to the acute margin of the heart.  $RCA_{AM}$ : a point at the acute margin of the heart.

## Left Coronary

The velocity of the left coronary landmarks over the cardiac cycle is plotted in Figure 6.5. The curves are similar in shape to those seen for the right coronary landmarks, but the left coronary velocities are smaller in magnitude. In addition, the left coronary tree shows less variation in the peak velocities between systole, diastolic filling, and atrial contraction for a given landmark.

The peak values for the three high velocity phases of the cardiac cycle are summarized in Table 6.5 for seven patients. The inter-patient range of peak velocity was 21.4-68.4 mm/s during systole, 16.6-73.4 mm/s during early diastole, and 12.0-109.1 mm/s during the atrial contraction.

The left circumflex had higher velocities than the LM ostium during the cardiac cycle. The peak velocity of LCx<sub>5</sub> during systole was 56.5±10.3 mm/s compared with peak velocity at LM<sub>0</sub> of 34.5±8.8 mm/s (P<0.0005, Bonferroni t-test with six comparisons). The same statistical relationship existed for the rapid filling phase of early diastole (P<0.004), and the atrial contraction (P<0.0005).

The minimum velocities at end-systole and in diastasis are summarized in Table 6.6. The inter-patient range of minimum velocity was 0.8-17.3 mm/s at end-systole, and 1.3-9.8 mm/s during diastasis. During the quiescent period at end-systole, the circumflex velocity was higher than the other three landmarks' velocities (P<0.001, Bonferroni t-test with six comparisons).

The minimum velocities during end-systole and in diastasis were not statistically different, but were significantly lower than the the peak velocities during systole, early-diastole, and atrial contraction.

Table 6.5: Maximum 3D velocity of the left coronary tree during the cardiac contraction in millimeters per second (mm/s). The results are the mean and standard deviation for seven patients.

Left Coronary Landmark	Maximum Velocity: Cardiac Contraction		
	Systole (mm/s)	Diastolic Filling (mm/s)	Atrial Contraction (mm/s)
LM <sub>O</sub>	34.5 ± 8.8	27.9 ± 9.2	29.1 ± 13.8
LM <sub>B</sub>	39.1 ± 5.4	32.6 ± 11.3	31.5 ± 13.9
LAD <sub>5</sub>	47.5 ± 9.3	35.6 ± 12.6	36.8 ± 14.3
LCx <sub>5</sub>	56.4 ± 10.1	46.7 ± 17.9	51.3 ± 28.3

Table 6.6: Minimum 3D velocity of the left coronary tree during the cardiac contraction in millimeters per second (mm/s). The results are the mean and standard deviation for seven patients.

Left Coronary Landmark	Minimum Velocity: Cardiac Contraction	
	End-Systole (mm/s)	Diastasis (mm/s)
LM <sub>O</sub>	3.7 ± 2.3	5.3 ± 2.8
LM <sub>B</sub>	4.5 ± 2.0	5.2 ± 2.2
LAD <sub>5</sub>	5.2 ± 2.7	3.6 ± 1.7
LCx <sub>5</sub>	10.9 ± 4.7	4.4 ± 2.6

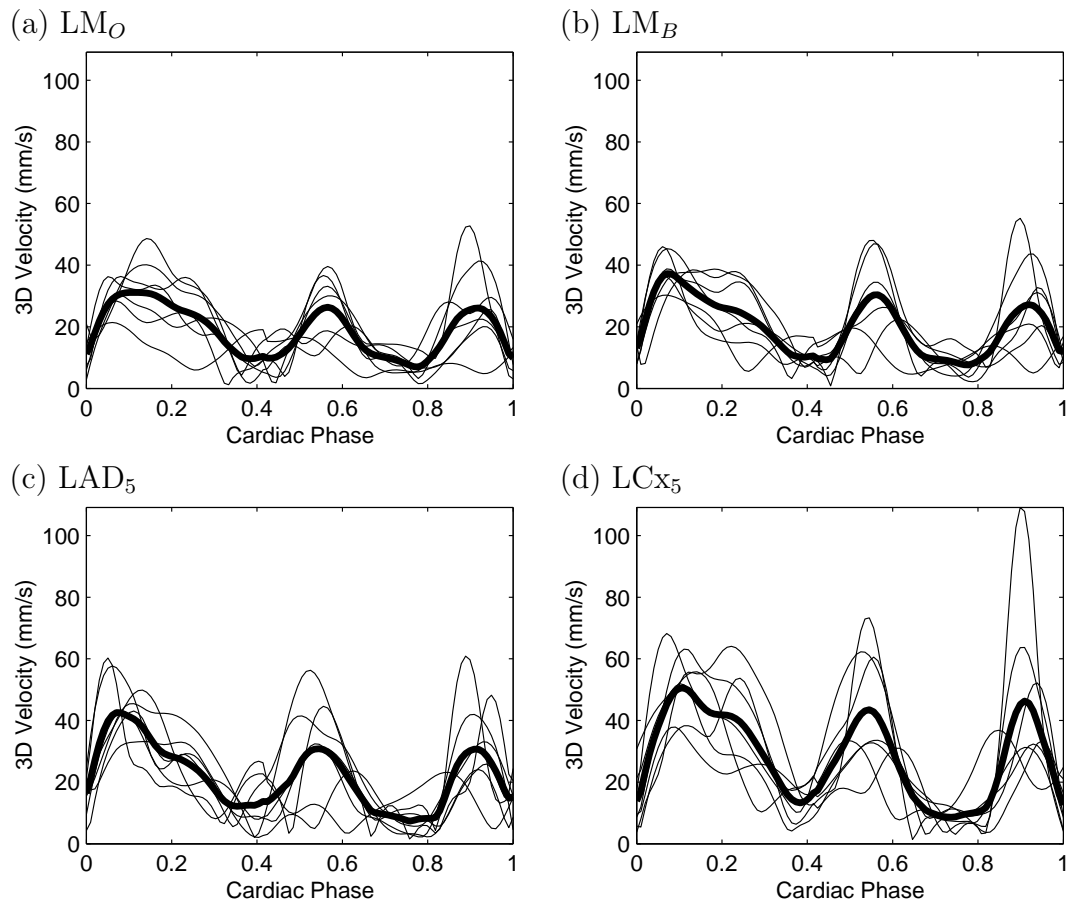


Figure 6.5: Velocity of the left coronary tree during the cardiac contraction (at end-expiration). The plot shows individual results for seven patients (thin lines) and the mean velocity (thick line). LM<sub>O</sub>: the LM origin. LM<sub>B</sub>: the LM bifurcation. LAD<sub>5</sub>: a point on the LAD 5 cm from the LM ostium. LCx<sub>5</sub>: a point on the LCx 5 cm from the LM ostium.

### 6.2.3 Rest Period

#### Right Coronary Tree

Figure 6.6 shows the rest period duration of the right coronary artery for four patients as a function of the cardiac phase. In this example, the rest period was the amount of time during which the 3D motion of the artery was less than 1 mm. The plot suggest that there are two phases of the cardiac cycle during which the motion of the heart is small: (1) at end-systole, and (2) at mid-diastole. The location of these rest periods coincide with the low velocity phases of the cardiac cycle measured in Section 6.2.2.

For an allowed 3D motion of 1 mm, the mean end-systolic rest period duration was  $76.1 \pm 33.8$  ms (range, 47-115 ms). The rest period was centered at  $\chi = 0.41 \pm 0.02$  (range, 0.39-0.43). The mean mid-diastolic rest period duration was  $64.6 \pm 41.6$  ms (range, 21-116 ms) and it was centered at  $\chi = 0.72 \pm 0.04$  (range, 0.68-0.77).

Decreasing the amount of motion which is acceptable during the rest period, reduces the duration of the rest period. For an allowed 3D motion of 0.5 mm, the mean end-systolic rest period duration was  $40.6 \pm 20.7$  ms (range, 28-71 ms). The rest period was centered at  $\chi = 0.41 \pm 0.02$  (range, 0.40-0.44). The mean mid-diastolic rest period duration was  $29.8 \pm 19.0$  ms (range, 7-53 ms) and it was centered at  $\chi = 0.73 \pm 0.03$  (range, 0.70-0.77).

Figure 6.7 shows the relationship between the allowed 3D motion and the right coronary rest period for a range of allowed 3D motions. The raw results are provided in Table 6.7.

#### Left Coronary Tree

Figure 6.8 shows the rest period duration of the left coronary tree for seven patients as a function of the cardiac phase. Qualitatively, the two rest periods are found at the same position as seen for the right coronary artery: at end-systole and at mid-diastole.

For an allowed 3D motion of 0.5 mm, the mean end-systolic rest period duration was  $41.3 \pm 15.1$  ms (range, 29-71 ms). The rest period was centered at  $\chi = 0.37 \pm 0.05$  (range, 0.30-0.45). The mean mid-diastolic rest period duration was  $55.3 \pm 21.5$  ms

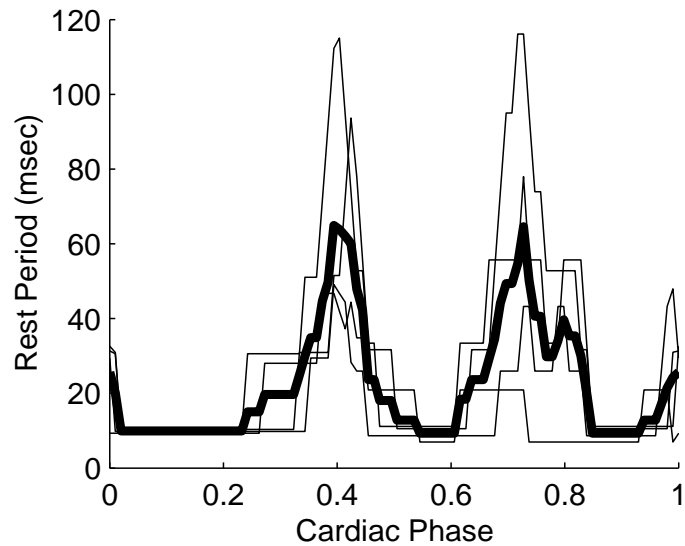


Figure 6.6: Right coronary rest period duration during the cardiac contraction (at end-expiration). The maximum allowed 3D motion of the artery is one millimeter. The graph shows individual results for four patients (thin lines) and the mean rest period (thick line).

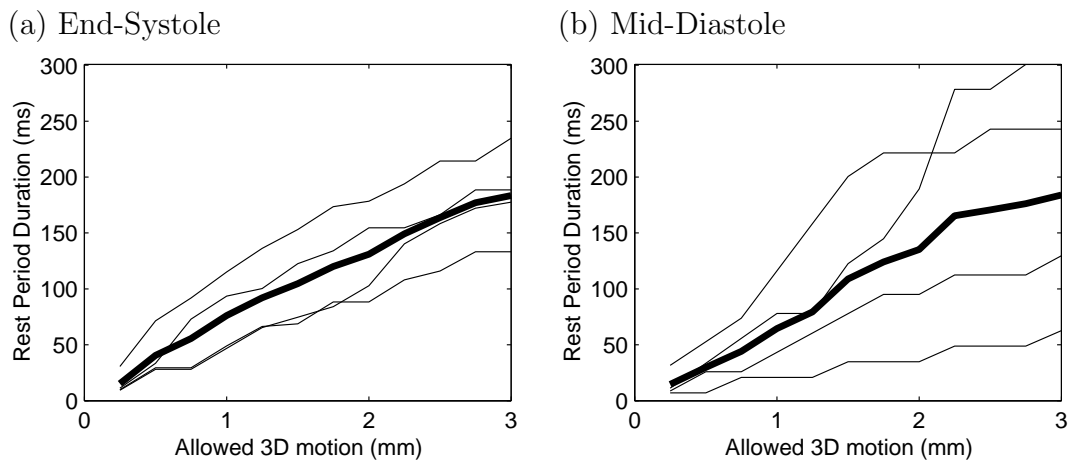


Figure 6.7: Right coronary rest period duration during the cardiac contraction as a function of the maximum allowed 3D motion at (a) end-systole and (b) mid-diastole. The graph shows individual results for four patients (thin lines) and their mean (thick line).

Table 6.7: Cardiac contraction: right coronary rest period duration and position in the cardiac cycle. The range of values is provided in parentheses below each mean and standard deviation.

Allowed 3D motion (mm)	Duration of Rest Period (ms)		Center of Rest Period $\chi(\times 100)$	
	Systolic	Diastolic	Systolic	Diastolic
0.25	$15.2 \pm 10.3$ ( 9 - 31)	$14.6 \pm 11.5$ ( 7 - 32)	$37.9 \pm 8.7$ ( 31 - 49)	$70.2 \pm 0.5$ ( 70 - 71)
0.5	$40.6 \pm 20.7$ ( 28 - 71)	$29.8 \pm 19.0$ ( 7 - 53)	$41.0 \pm 2.0$ ( 40 - 44)	$73.2 \pm 2.8$ ( 70 - 77)
0.75	$55.6 \pm 31.9$ ( 28 - 92)	$44.1 \pm 25.1$ ( 21 - 74)	$40.1 \pm 2.3$ ( 38 - 43)	$72.7 \pm 3.3$ ( 69 - 76)
1	$76.1 \pm 33.8$ ( 47 - 115)	$64.6 \pm 41.6$ ( 21 - 116)	$40.8 \pm 1.7$ ( 39 - 43)	$72.4 \pm 3.7$ ( 68 - 77)
1.25	$92.1 \pm 33.6$ ( 65 - 136)	$79.4 \pm 57.8$ ( 21 - 158)	$40.8 \pm 1.7$ ( 39 - 43)	$71.1 \pm 4.4$ ( 65 - 74)
1.5	$104.8 \pm 40.3$ ( 69 - 153)	$109.0 \pm 70.8$ ( 35 - 201)	$40.8 \pm 1.5$ ( 40 - 43)	$74.5 \pm 5.1$ ( 69 - 81)
1.75	$120.0 \pm 42.2$ ( 84 - 174)	$124.1 \pm 79.1$ ( 35 - 222)	$40.2 \pm 1.3$ ( 39 - 42)	$72.0 \pm 2.8$ ( 69 - 75)
2	$131.1 \pm 42.5$ ( 88 - 178)	$135.3 \pm 85.8$ ( 35 - 222)	$41.0 \pm 0.7$ ( 41 - 42)	$72.2 \pm 3.7$ ( 68 - 76)
2.25	$149.2 \pm 35.6$ ( 108 - 194)	$165.4 \pm 103.9$ ( 49 - 279)	$40.5 \pm 1.0$ ( 40 - 42)	$73.4 \pm 3.3$ ( 69 - 76)
2.5	$163.7 \pm 40.3$ ( 116 - 214)	$170.6 \pm 108.1$ ( 49 - 279)	$40.8 \pm 1.0$ ( 40 - 42)	$73.1 \pm 3.5$ ( 68 - 76)
2.75	$177.1 \pm 34.0$ ( 133 - 214)	$176.2 \pm 115.9$ ( 49 - 301)	$40.8 \pm 1.0$ ( 40 - 42)	$72.9 \pm 3.3$ ( 68 - 76)
3	$183.6 \pm 41.7$ ( 133 - 235)	$184.0 \pm 107.6$ ( 63 - 301)	$40.5 \pm 1.3$ ( 39 - 42)	$73.0 \pm 3.5$ ( 68 - 76)

(range, 36-97 ms) and it was centered at  $\chi=0.75\pm0.06$  (range, 0.63-0.82).

Increasing the amount of motion which is acceptable during the rest period, also increases the duration of the rest period. For an allowed 3D motion of 1 mm, the mean end-systolic rest period duration was  $79.9\pm25.4$  ms (range, 52-131 ms). The rest period was centered at  $\chi=0.38\pm0.04$  (range, 0.30-0.43). The mean mid-diastolic rest period duration was  $112.1\pm42.4$  ms (range, 65-183 ms) and it was centered at  $\chi=0.74\pm0.06$  (range, 0.63-0.81).

Figure 6.9 shows the relationship between the allowed 3D motion and the left coronary rest period for a range of allowed 3D motions. The raw results are provided in Table 6.8.

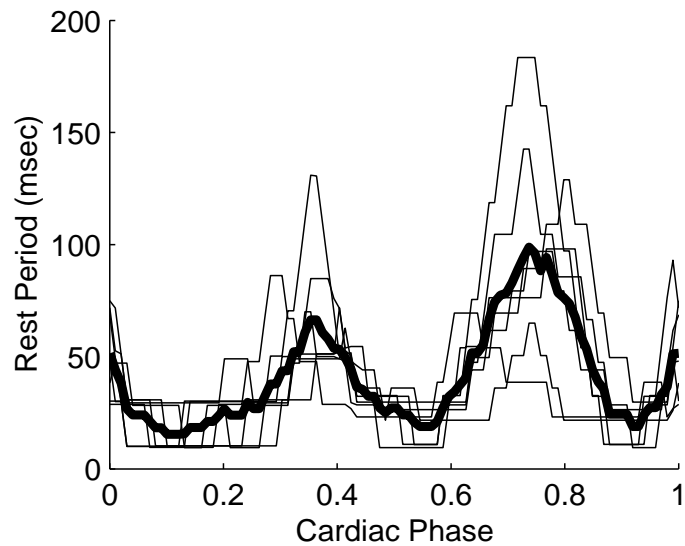


Figure 6.8: Left coronary rest period duration during the cardiac contraction (at end-expiration). The maximum allowed 3D motion of the arteries is one millimeter. The graph shows individual results for seven patients (thin lines) and the mean rest period (thick line).

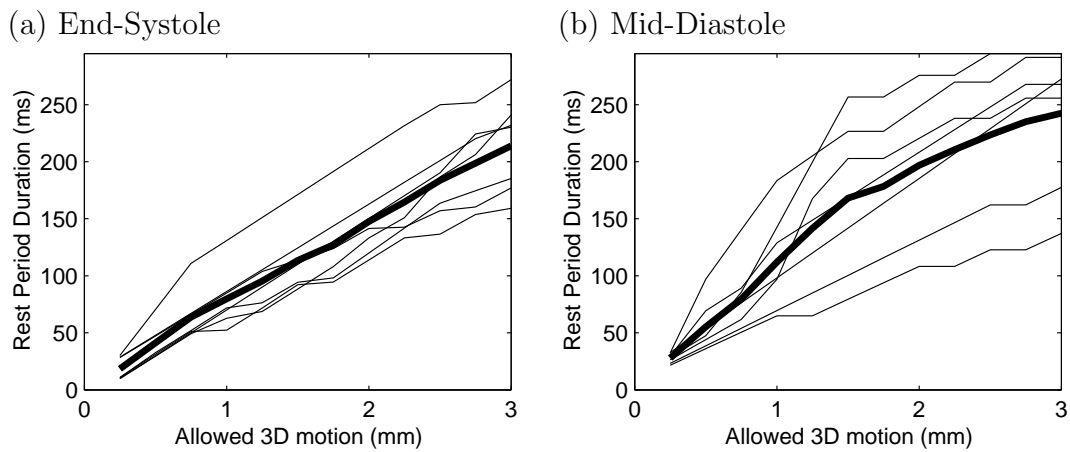


Figure 6.9: Left coronary rest period duration during the cardiac contraction as a function of the maximum allowed 3D motion at (a) end-systole and (b) mid-diastole. The graph shows individual results for seven patients (thin lines) and their mean (thick line).

Table 6.8: Cardiac contraction: left coronary rest period duration and position in the cardiac cycle. The range of values is provided in parentheses below each mean and standard deviation.

Allowed 3D motion (mm)	Duration of Rest Period (ms)		Center of Rest Period $\chi(\times 100)$	
	Systolic	Diastolic	Systolic	Diastolic
0.25	$18.4 \pm 10.0$ ( 10 - 30)	$27.8 \pm 4.3$ ( 22 - 33)	$37.9 \pm 8.2$ ( 30 - 49)	$74.6 \pm 6.0$ ( 63 - 81)
0.5	$41.3 \pm 15.1$ ( 29 - 71)	$55.3 \pm 21.5$ ( 36 - 97)	$37.2 \pm 5.2$ ( 30 - 45)	$75.3 \pm 6.3$ ( 63 - 82)
0.75	$63.7 \pm 22.1$ ( 49 - 111)	$79.7 \pm 30.7$ ( 51 - 140)	$37.1 \pm 4.0$ ( 30 - 43)	$74.9 \pm 5.8$ ( 63 - 81)
1	$79.9 \pm 25.4$ ( 52 - 131)	$112.1 \pm 42.4$ ( 65 - 183)	$37.6 \pm 4.2$ ( 30 - 42)	$74.4 \pm 5.7$ ( 63 - 81)
1.25	$95.3 \pm 28.7$ ( 69 - 151)	$141.6 \pm 54.3$ ( 65 - 205)	$37.3 \pm 3.9$ ( 31 - 43)	$74.1 \pm 5.3$ ( 64 - 80)
1.5	$113.5 \pm 28.6$ ( 88 - 171)	$168.1 \pm 65.4$ ( 79 - 257)	$37.6 \pm 4.4$ ( 31 - 44)	$74.2 \pm 5.0$ ( 64 - 79)
1.75	$127.1 \pm 33.4$ ( 94 - 191)	$178.3 \pm 58.4$ ( 94 - 257)	$38.0 \pm 4.4$ ( 31 - 44)	$74.1 \pm 4.9$ ( 64 - 79)
2	$147.6 \pm 32.8$ ( 114 - 212)	$196.8 \pm 60.3$ ( 108 - 276)	$37.6 \pm 4.4$ ( 31 - 44)	$73.8 \pm 4.5$ ( 65 - 79)
2.25	$164.6 \pm 34.2$ ( 133 - 232)	$210.6 \pm 62.4$ ( 108 - 276)	$37.6 \pm 4.1$ ( 31 - 43)	$73.7 \pm 4.7$ ( 64 - 78)
2.5	$183.6 \pm 36.7$ ( 137 - 250)	$223.5 \pm 60.6$ ( 123 - 295)	$37.7 \pm 3.9$ ( 31 - 43)	$73.5 \pm 4.5$ ( 64 - 78)
2.75	$198.7 \pm 36.7$ ( 154 - 252)	$235.1 \pm 66.4$ ( 123 - 295)	$37.6 \pm 3.6$ ( 31 - 42)	$73.5 \pm 4.2$ ( 65 - 78)
3	$213.8 \pm 40.5$ ( 159 - 272)	$242.4 \pm 60.8$ ( 137 - 295)	$38.3 \pm 3.8$ ( 32 - 43)	$73.3 \pm 4.4$ ( 65 - 78)

## 6.3 Results : Respiratory Motion

In the four right coronary datasets, the patients had a mean respiratory rate of  $14.6 \pm 2.2$  breaths per minute (range, 12.5-17.6 breaths per minute). In the seven left coronary datasets, the patients had a mean respiratory rate of  $15.7 \pm 4.2$  breaths per minute (range, 9.4-21.4 breaths per minute).

### 6.3.1 Displacement

#### Right Coronary

The displacement of the RCA ostium over the respiratory cycle in four patients is shown in Figure 6.10. The shape of the 3D displacement curve has a minimum at end expiration  $\rho=0$ , and a maximum near  $\rho=\pm 1$ . Individual differences in the patient's breathing pattern affects the shape of these curves.

The maximum 3D displacement of the RCA ostium over the respiratory cycle, representing the motion from end expiration to end inspiration during tidal breathing, was  $5.0 \pm 1.3$  mm (range, 3.3-6.1 mm). At  $RCA_{(0.5)AM}$ , the tidal respiratory displacement was  $6.4 \pm 1.9$  mm (range, 3.8-8.4 mm). At the distal  $RCA_{AM}$  landmark, the tidal respiratory displacement was  $7.2 \pm 2.2$  mm (range, 4.6-9.7 mm). Larger maximum displacements were observed distally along the RCA due to respiration, with the displacement at  $RCA_{AM}$  statistically larger than at  $RCA_O$  ( $P < 0.007$ , Bonferroni t-test with three comparisons).

A summary of maximum 1D and 3D displacements over the respiratory cycle, at different points along the RCA, is presented in Table 6.9. The motion was primarily in the IS direction, but varied considerably both between patients and between the three landmarks. From end-expiration to end-inspiration, the motion was consistently directed towards the patient's feet. The direction of motion in the LR and AP axes was more variable. At the RCA ostium, there was almost no directional preference, while at  $RCA_{AM}$  the motion was, on average, directed towards the right and anterior.

At the RCA ostium,  $55 \pm 16\%$  of the respiratory motion was found in the IS axis,  $30 \pm 16\%$  in the LR axis and  $14 \pm 16\%$  in the AP axis. At  $RCA_{AM}$  the IS motion still

Table 6.9: Maximum displacement of the right coronary artery during a tidal breath (at diastasis). The results are the mean and standard deviation for four patients. Positive displacements are toward the left, inferior, and posterior, respectively.

Right Coronary Landmark	Displacement: Respiratory Motion			
	3D (mm)	LR (mm)	IS (mm)	AP (mm)
RCA <sub>O</sub>	5.0 ± 1.3	-0.5 ± 2.8	4.1 ± 1.6	-0.4 ± 1.3
RCA <sub>(.5)AM</sub>	6.4 ± 1.9	-0.3 ± 3.4	5.1 ± 2.1	-1.0 ± 2.5
RCA <sub>AM</sub>	7.2 ± 2.2	-1.3 ± 1.6	5.9 ± 3.1	-2.1 ± 2.7

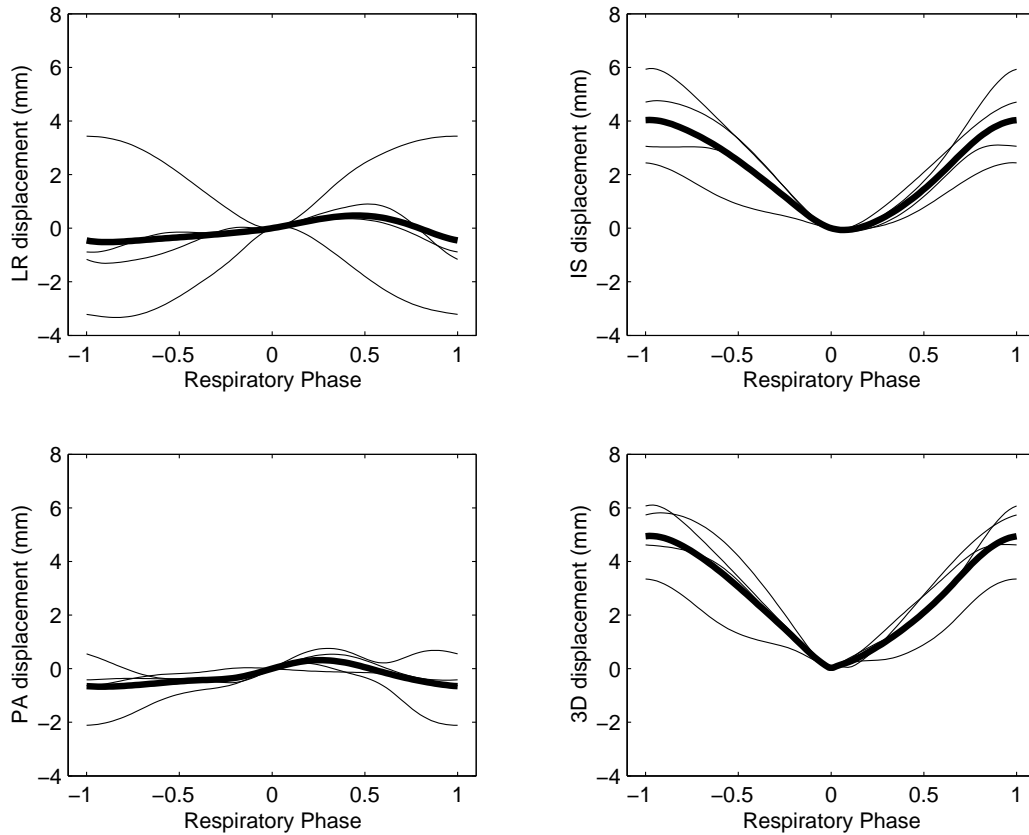


Figure 6.10: Displacement of the RCA origin during a tidal breath (at diastasis). The plots show individual results for four patients (thin lines) and the mean displacement (thick lines). The 1D displacements are with respect to the patient’s left-right (LR), inferior-superior (IS), and posterior-anterior (PA) axes. Positive displacements are towards the left, inferior, and posterior, respectively. The magnitude of the 3D displacement is shown in the bottom right plot.

accounted for  $54\pm 20\%$  of the total motion. But the motion in the other two axes flipped in importance, with the LR motion accounting for  $17\pm 9\%$  and the AP motion for  $29\pm 21\%$  of the total motion.

### Left Coronary

The displacement of the left main ostium over the respiratory cycle in seven patients is shown in Figure 6.11. The shape and magnitude of the displacement curves are similar to those seen for the right coronary ostium.

The maximum 3D displacement of the LM ostium over the respiratory cycle, representing the motion from end expiration to end inspiration during tidal breathing, was  $4.6\pm 1.4$  mm (range, 3.1-6.8 mm). At  $LAD_5$ , the tidal respiratory displacement was  $5.6\pm 2.1$  mm (range, 2.9-9.3 mm). At  $LCx_5$ , the tidal respiratory displacement was  $6.3\pm 1.6$  mm (range, 4.4-8.5 mm). The displacement at  $LCx_5$  was statistically larger than at  $LM_0$  ( $P < 0.0001$ ) and at  $LM_B$  ( $P < 0.002$ , Bonferroni t-test with six comparisons). The spatial variation in displacement suggests that the motion due to respiration is more complex than a simple 3D translation.

A summary of maximum 1D and 3D displacements over the respiratory cycle, at different points in the left coronary tree, is presented in Table 6.10. Similar to the right coronary motion, the left coronary landmarks consistently moved inferiorly during inspiration. The LR motion was highly variable, both in magnitude and direction. At each landmark, the patient averaged motion was directed anteriorly.

At the LM ostium,  $66\pm 19\%$  of the respiratory motion was found in the IS axis,  $22\pm 18\%$  in the LR axis and  $12\pm 9\%$  in the AP axis. At the distal landmarks, the relative contributions of the directional motion remained similar. At  $LAD_5$ , the contribution was  $57\pm 16$  in the IS axis,  $28\pm 14$  in the LR axis, and  $15\pm 9$  in the AP axis. At  $LCx_5$ , the percentages were  $64\pm 17$  in the IS axis,  $20\pm 13$  in the LR axis, and  $16\pm 10$  in the AP axis.

Table 6.10: Maximum displacement of the left coronary artery during a tidal breath (at diastasis). The results are the mean and standard deviation for seven patients. Positive displacements are toward the left, inferior, and posterior, respectively.

Left Coronary Landmark	Displacement: Respiratory Motion			
	3D (mm)	LR (mm)	IS (mm)	AP (mm)
LM	$4.6 \pm 1.4$	$-0.4 \pm 3.0$	$4.1 \pm 1.0$	$-0.8 \pm 1.1$
$LM_B$	$5.0 \pm 1.6$	$-0.1 \pm 3.0$	$4.3 \pm 1.1$	$-0.8 \pm 1.4$
$LAD_5$	$5.6 \pm 2.1$	$0.1 \pm 3.5$	$4.7 \pm 1.8$	$-0.7 \pm 1.9$
$LCx_5$	$6.3 \pm 1.6$	$0.3 \pm 2.8$	$5.6 \pm 1.5$	$-0.6 \pm 1.9$

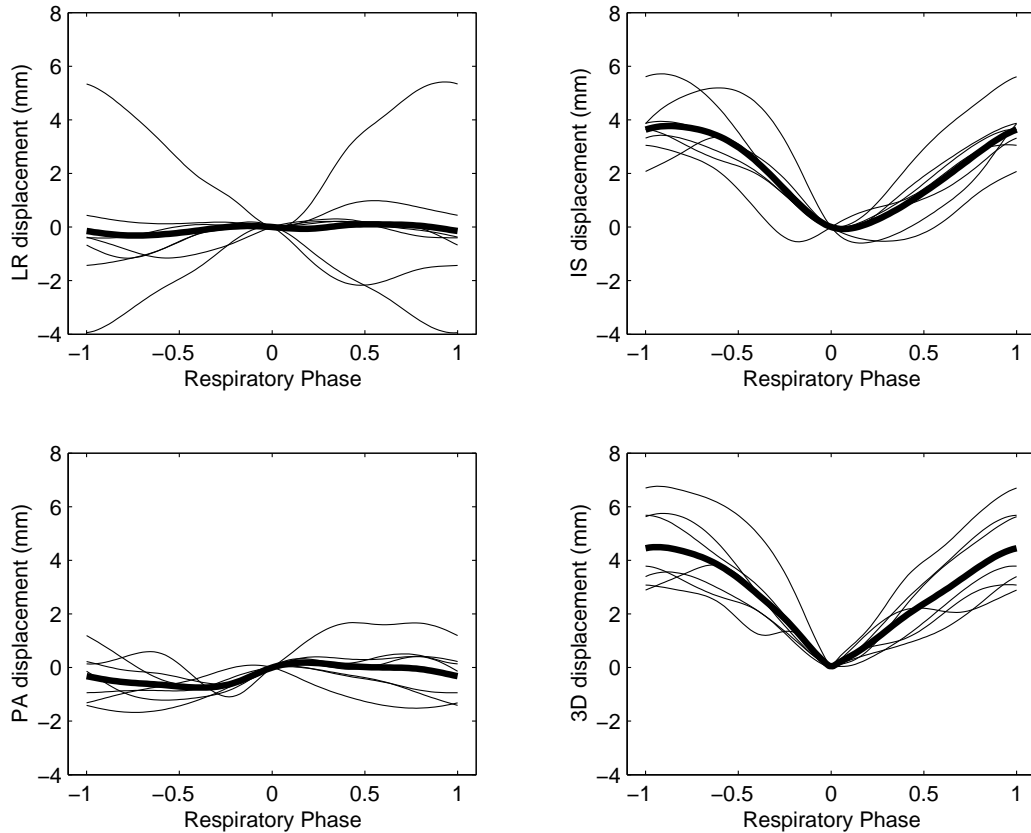


Figure 6.11: Displacement of the LM origin during a tidal breath (at diastasis). The plots show individual results for seven patients (thin lines) and the mean displacement (thick lines). The 1D displacements are with respect to the patient’s left-right (LR), inferior-superior (IS), and posterior-anterior (PA) axes. Positive displacements are towards the left, inferior, and posterior, respectively. The magnitude of the 3D displacement is shown in the bottom right plot.

## 6.3.2 Velocity

### Right Coronary

The velocity of the RCA landmarks during the respiratory cycle is plotted in Figure 6.12. Low velocity regions are observed at end-inspiration ( $\rho=\pm 1$ ) and at end-expiration ( $\rho=0$ ). The velocity is higher during the expiratory ( $-1 < \rho < 0$ ) and inspiratory ( $0 < \rho < 1$ ) maneuvers.

At  $RCA_0$  the mean velocity was  $2.8\pm 0.6$  mm/s during inspiration, and  $2.0\pm 0.4$  mm/s during expiration. At  $RCA_{AM}$  the values were  $4.0\pm 0.9$  mm/s and  $2.9\pm 0.6$  mm/s. The difference between mean inspiratory and expiratory velocities is due to differences in the duration of the inspiratory and expiratory maneuvers since the displacement during the two phases is nearly equal in magnitude.

The distal  $RCA_{AM}$  landmark had a higher mean expiratory velocity than  $RCA_0$  ( $P < 0.004$ , Bonferroni t-test with three comparisons). The mean inspiratory velocity was also higher at  $RCA_{AM}$  than  $RCA_0$  ( $P < 0.006$ , Bonferroni t-test with three comparisons). Since the duration of the respiratory maneuver is the same as the proximal landmarks, the increased mean velocities at distal landmarks can be attributed to larger motion of these distal landmarks due to respiration. This is consistent with the displacements measured in Section 6.3.1.

The peak expiratory velocity at the distal landmark  $RCA_{AM}$  (mean,  $6.4\pm 1.7$  mm/s) was significantly higher than the peak expiratory velocity at the RCA ostium (mean,  $4.5\pm 1.6$  mm/s,  $P < 0.008$ , Bonferroni t-test with three comparisons). The peak expiratory velocities measured on the right coronary artery ranged between 3.3-8.6 mm/s in the four patients.

Similarly, the peak inspiratory velocity at the  $RCA_{AM}$  (mean,  $9.0\pm 3.1$  mm/s) was higher than the inspiratory velocity at the RCA ostium (mean,  $6.6\pm 1.3$  mm/s). The range of peak inspiratory velocities was 5.3-13.5 mm/s. The peak inspiratory and expiratory velocities for different points on the right coronary are summarized in Table 6.11. The minimum velocity measured at end-inspiration and end-expiration ranged between 0.0-1.4 mm/s.

Table 6.11: Maximum 3D velocity of the right coronary artery during a tidal breath in millimeters per second (mm/s). The results are the mean and standard deviation for four patients.

Right Coronary Landmark	Maximum Velocity: Respiratory Motion	
	Expiration (mm/s)	Inspiration (mm/s)
$RCA_O$	$4.5 \pm 1.6$	$6.6 \pm 1.3$
$RCA_{(0.5)AM}$	$5.7 \pm 1.6$	$8.0 \pm 2.5$
$RCA_{AM}$	$6.4 \pm 1.7$	$9.0 \pm 3.1$

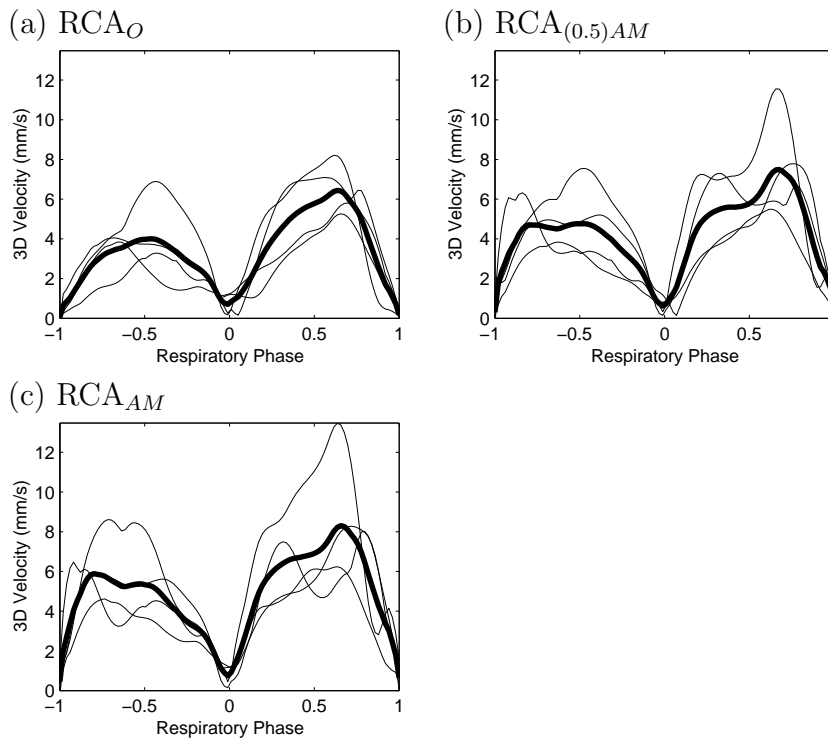


Figure 6.12: Velocity of the right coronary artery during a tidal breath in millimeters per second (mm/s). The plot shows individual results for four patients (thin lines) and the mean velocity (thick line).  $RCA_O$ : the RCA origin.  $RCA_{(0.5)AM}$ : a point approximately one-half the distance to the acute margin of the heart.  $RCA_{AM}$ : a point at the acute margin of the heart.

## Left Coronary

The velocity of the left coronary landmarks during the respiratory cycle is plotted in Figure 6.13. The shape of the velocity profiles is consistent with those seen for the right coronary artery.

At each landmark there was a statistically significant difference between mean expiratory and inspiratory velocity:

- $LM_O$ : the mean expiratory velocity ( $2.1 \pm 1.1$  mm/s) was significantly less than the mean inspiratory velocity ( $3.0 \pm 1.2$  mm/s,  $P < 0.004$ , t-test for paired samples).
- $LM_B$ : the mean expiratory velocity ( $2.2 \pm 1.2$  mm/s) was significantly less than the mean inspiratory velocity ( $3.2 \pm 1.2$  mm/s,  $P < 0.004$ , t-test for paired samples).
- $LAD_5$ : the mean expiratory velocity ( $2.6 \pm 1.4$  mm/s) was significantly less than the mean inspiratory velocity ( $3.7 \pm 1.4$  mm/s,  $P < 0.005$ , t-test for paired samples).
- $LCX_5$ : the mean expiratory velocity ( $2.8 \pm 1.3$  mm/s) was significantly less than the mean inspiratory velocity ( $4.2 \pm 1.6$  mm/s,  $P < 0.01$ , t-test for paired samples).

As described for the right coronary artery, the difference between mean inspiratory and expiratory velocities is due to differences in the duration of the inspiratory and expiratory maneuvers.

Distal landmarks had higher mean velocities than proximal ones. During inspiration, the mean inspiratory velocity at  $LM_0$  was significantly lower than at  $LCX_5$  ( $P < 0.001$ , Bonferroni t-test with six comparisons). This spatial relationship was also observed during expiration. The mean expiratory velocity at  $LM_0$  was significantly lower than the mean  $LCX_5$  velocity ( $P < 0.001$ , Bonferroni t-test with six comparisons).

The peak expiratory velocities measured on the left coronary artery ranged between 2.8-15.3 mm/s in the seven patients. The range of peak inspiratory velocities

Table 6.12: Maximum 3D velocity of the left coronary artery during a tidal breath in millimeters per second (mm/s). The results are the mean and standard deviation for seven patients.

Right Coronary Landmark	Respiratory Motion	
	Expiration (mm/s)	Inspiration (mm/s)
$LM_O$	$5.5 \pm 2.0$	$6.0 \pm 1.8$
$LM_B$	$5.7 \pm 2.4$	$6.3 \pm 2.0$
$LAD_5$	$7.6 \pm 3.9$	$7.8 \pm 3.0$
$LCx_5$	$6.9 \pm 3.1$	$8.5 \pm 4.3$

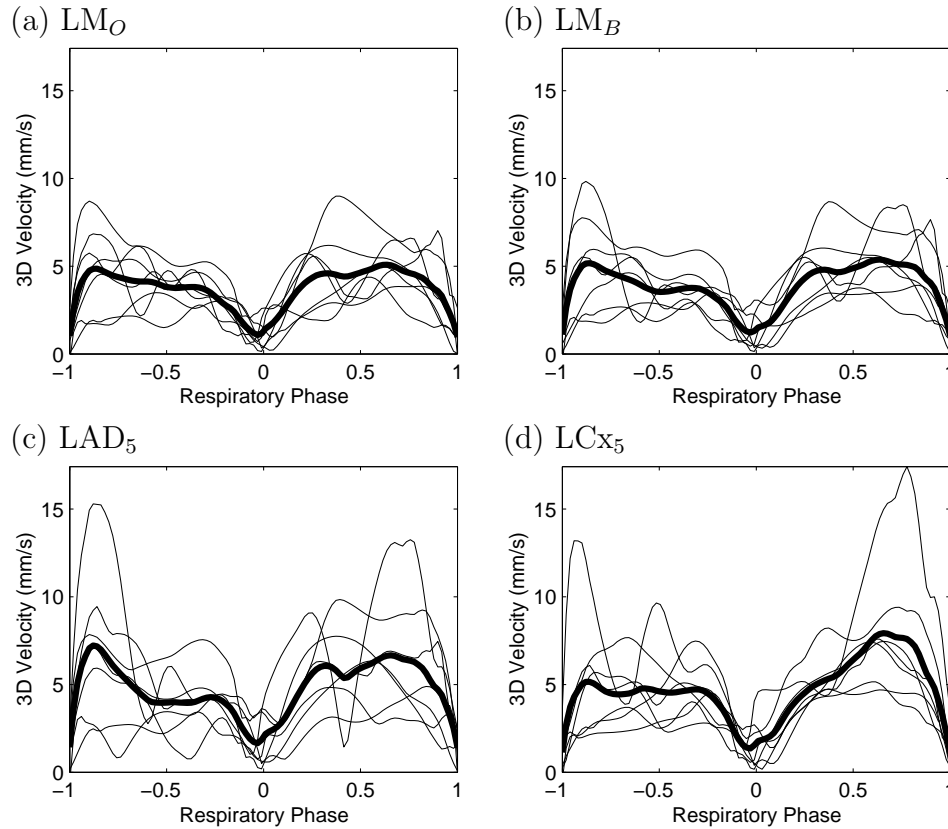


Figure 6.13: Velocity of the left coronary artery during a tidal breath in millimeters per second (mm/s). The plot shows individual results for seven patients (thin lines) and the mean velocity (thick line).  $LM_O$ : the LM origin.  $LM_B$ : the LM bifurcation.  $LAD_5$ : a point on the LAD 5 cm from the LM ostium.  $LCx_5$ : a point on the LCx 5 cm from the LM ostium.

was 3.8-17.4 mm/s. The peak inspiratory and expiratory velocities for different points on the left coronary tree are summarized in Table 6.12. The minimum velocity measured at end-inspiration and end-expiration ranged between 0.0-3.4 mm/s.

### 6.3.3 Rest Period

#### Right Coronary Tree

Figure 6.14 shows the rest period duration as a function of the respiratory cycle for the right coronary artery in four patients. In this example, the rest period was measured with an allowed 3D motion of 1 mm. The traces suggest the existence of two points in the respiratory cycle where the motion of the heart due to respiration is minimized: end-expiration ( $\rho=0$ ) and end-inspiration ( $\rho=\pm 1$ ). The location of these rest periods coincide with the low velocity phases of the respiratory cycle measured in Section 6.3.2.

For an allowed 3D motion of 1 mm, the mean end-expiration rest period duration was  $1065 \pm 320$  ms (range, 844-1536 ms). As a percentage of the patients' respiratory period, the mean end-expiration rest period duration was  $26 \pm 8\%$  (range, 18-37%). The mean end-inspiration rest period duration was  $655 \pm 227$  ms (range, 415-939 ms), or  $16 \pm 8\%$  (range, 9-28%).

Decreasing the amount of motion which is acceptable during the rest period, reduces the duration of the rest period. For an allowed 3D motion of 0.5 mm, the mean end-expiration rest period duration was  $685 \pm 340$  ms (range, 430-1161 ms), or  $17 \pm 8\%$  (range, 9-28%). The mean end-inspiration rest period duration was  $383 \pm 167$  ms (range, 196-595 ms), or  $10 \pm 6\%$  (range, 4-18%).

Figure 6.15 shows the relationship between the allowed 3D motion and the right coronary rest period for a range of allowed 3D motions. The raw results are provided in Table 6.13.

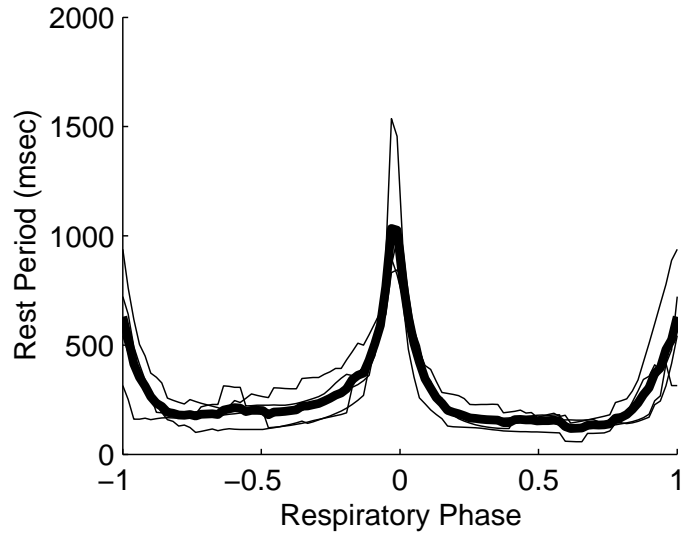


Figure 6.14: Right coronary rest period duration during a tidal breath. The cardiac cycle is held constant at mid-diastole. The maximum allowed 3D motion of the artery is one millimeter. The graph shows individual results for four patients (thin lines) and the mean rest period (thick line).

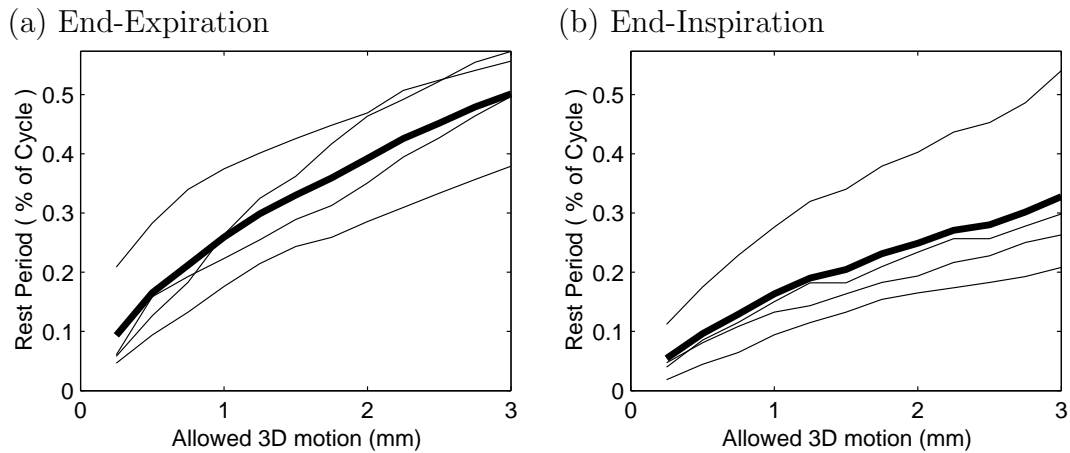


Figure 6.15: Right coronary rest period duration during a tidal breath as a function of the maximum allowed 3D motion at (a) end-expiration and (b) end-inspiration. The graph shows individual results for four patients (thin lines) and their mean (thick line).

Table 6.13: Tidal breathing: right coronary rest period duration in milliseconds (msec) and as a percentage of the respiratory period. The cardiac cycle is held constant at mid-diastole. The range of values is provided in parentheses below each mean and standard deviation.

Allowed 3D motion (mm)	Duration of Rest Period			
	(ms)		(% of Cycle)	
	EE	EI	EE	EI
0.25	385 ± 315 ( 197 - 856)	212 ± 124 ( 82 - 381)	9 ± 8 ( 5 - 21)	5 ± 4 ( 2 - 11)
0.5	685 ± 340 ( 430 - 1161)	383 ± 167 ( 196 - 595)	17 ± 8 ( 9 - 28)	10 ± 6 ( 4 - 18)
0.75	875 ± 360 ( 622 - 1393)	515 ± 207 ( 284 - 777)	21 ± 9 ( 13 - 34)	13 ± 7 ( 6 - 23)
1	1065 ± 320 ( 844 - 1536)	655 ± 227 ( 415 - 939)	26 ± 8 ( 18 - 37)	16 ± 8 ( 9 - 28)
1.25	1225 ± 283 ( 1029 - 1646)	763 ± 267 ( 505 - 1087)	30 ± 8 ( 21 - 40)	19 ± 9 ( 11 - 32)
1.5	1354 ± 264 ( 1169 - 1746)	821 ± 255 ( 583 - 1156)	33 ± 8 ( 24 - 43)	20 ± 9 ( 13 - 34)
1.75	1468 ± 258 ( 1242 - 1838)	931 ± 277 ( 679 - 1288)	36 ± 9 ( 26 - 45)	23 ± 10 ( 15 - 38)
2	1604 ± 232 ( 1371 - 1924)	1003 ± 299 ( 726 - 1369)	39 ± 9 ( 29 - 47)	25 ± 11 ( 17 - 40)
2.25	1743 ± 248 ( 1485 - 2079)	1092 ± 328 ( 765 - 1484)	43 ± 9 ( 31 - 51)	27 ± 12 ( 17 - 44)
2.5	1851 ± 230 ( 1600 - 2150)	1127 ± 328 ( 804 - 1540)	45 ± 9 ( 33 - 52)	28 ± 12 ( 18 - 45)
2.75	1964 ± 216 ( 1712 - 2218)	1215 ± 354 ( 848 - 1653)	48 ± 9 ( 36 - 55)	30 ± 13 ( 19 - 49)
3	2059 ± 212 ( 1820 - 2281)	1316 ± 409 ( 916 - 1837)	50 ± 9 ( 38 - 57)	33 ± 15 ( 21 - 54)

### Left Coronary

Figure 6.16 shows the rest period duration as a function of the respiratory cycle for the left coronary tree in seven patients. In this example, the rest period was measured with an allowed 3D motion of 1 mm. The mean end-expiration rest period duration was  $1232 \pm 1172$  ms (range, 391-3629 ms). As a percentage of the patients' respiratory period, the mean end-expiration rest period duration was  $27 \pm 17\%$  (range, 9-57%). The mean end-inspiration rest period duration was  $444 \pm 273$  ms (range, 156-839 ms), or  $11 \pm 6\%$  (range, 5-21%).

Decreasing the amount of motion which is acceptable during the rest period, reduces the duration of the rest period. For an allowed 3D motion of 0.5 mm, the mean end-expiration rest period duration was  $834 \pm 925$  ms (range, 185-2727 ms), or  $18 \pm 14\%$  (range, 4-43%). The mean end-inspiration rest period duration was  $238 \pm 119$  ms (range, 102-438 ms), or  $6 \pm 3\%$  (range, 3-11%).

The raw results for a range of 3D motion limits are provided in Table 6.14. Figure 6.17 shows the relationship between the allowed 3D motion and the left coronary rest period for a range of allowed 3D motions.

For a 3D motion limit of 0.75 mm, the rest period duration at end-expiration (mean,  $23 \pm 16\%$  of the respiratory cycle) was significantly longer than at end-inspiration (mean,  $8 \pm 5\%$ ,  $P < 0.041$ , t-test for paired samples). The statistically significant difference was observed for each of the larger 3D motion cutoffs that were tested (up to 3 mm).

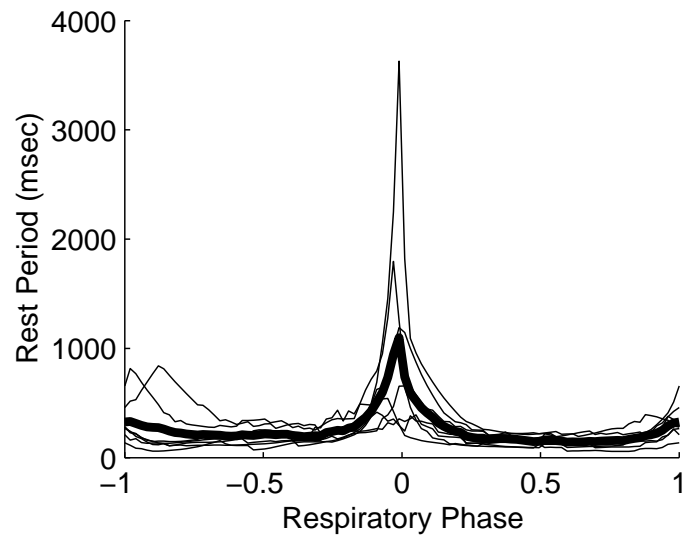


Figure 6.16: Left coronary rest period duration during a tidal breath. The cardiac cycle is held constant at mid-diastole. The maximum allowed 3D motion of the arteries is one millimeter. The graph shows individual results for seven patients (thin lines) and the mean rest period (thick line).

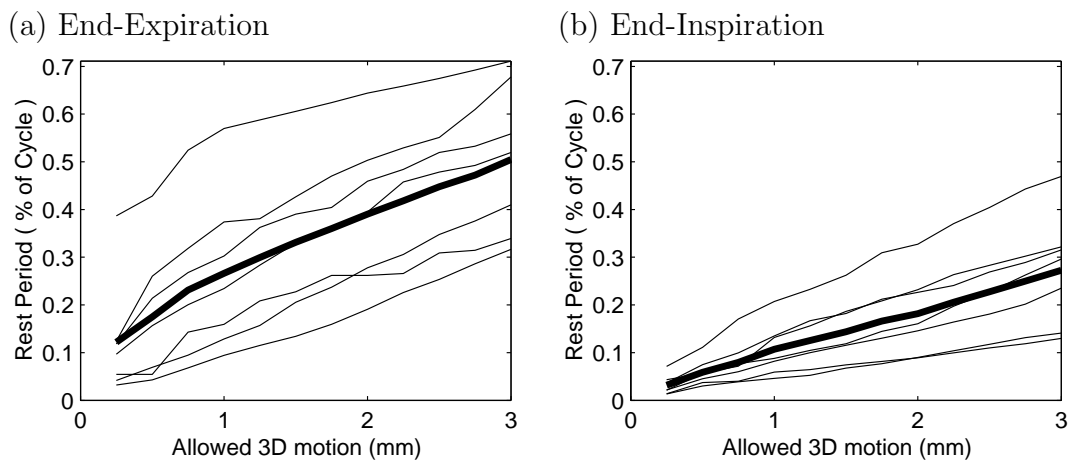


Figure 6.17: Left coronary rest period duration during a tidal breath as a function of the maximum allowed 3D motion at (a) end-expiration and (b) end-inspiration. The graph shows individual results for seven patients (thin lines) and their mean (thick line).

Table 6.14: Tidal breathing: left coronary rest period duration in milliseconds (msec) and as a percentage of the respiratory period. The cardiac cycle is held constant at mid-diastole. The range of values is provided in parentheses below each mean and standard deviation.

Allowed 3D motion (mm)	Duration of Rest Period			
	(ms)		(% of Cycle)	
	EE	EI	EE	EI
0.25	607 ± 837 ( 126 - 2462)	123 ± 77 ( 45 - 279)	12 ± 12 ( 3 - 39)	3 ± 2 ( 1 - 7)
0.5	834 ± 925 ( 185 - 2727)	238 ± 119 ( 102 - 438)	18 ± 14 ( 4 - 43)	6 ± 3 ( 3 - 11)
0.75	1080 ± 1093 ( 287 - 3340)	319 ± 186 ( 132 - 671)	23 ± 16 ( 7 - 52)	8 ± 5 ( 4 - 17)
1	1232 ± 1172 ( 391 - 3629)	444 ± 273 ( 156 - 839)	27 ± 17 ( 9 - 57)	11 ± 6 ( 5 - 21)
1.25	1354 ± 1166 ( 476 - 3743)	520 ± 316 ( 178 - 995)	30 ± 16 ( 12 - 59)	13 ± 6 ( 5 - 23)
1.5	1479 ± 1177 ( 591 - 3857)	600 ± 368 ( 229 - 1188)	33 ± 16 ( 13 - 61)	14 ± 7 ( 7 - 26)
1.75	1592 ± 1190 ( 702 - 3974)	689 ± 419 ( 261 - 1326)	36 ± 16 ( 16 - 62)	17 ± 8 ( 8 - 31)
2	1715 ± 1209 ( 841 - 4101)	755 ± 453 ( 307 - 1478)	39 ± 16 ( 19 - 64)	18 ± 9 ( 9 - 33)
2.25	1821 ± 1209 ( 903 - 4194)	855 ± 511 ( 354 - 1678)	42 ± 16 ( 23 - 66)	21 ± 10 ( 10 - 37)
2.5	1935 ± 1202 ( 1050 - 4296)	941 ± 543 ( 400 - 1802)	45 ± 15 ( 25 - 67)	23 ± 10 ( 11 - 40)
2.75	2040 ± 1238 ( 1069 - 4407)	1030 ± 579 ( 448 - 1925)	47 ± 15 ( 29 - 69)	25 ± 11 ( 12 - 44)
3	2175 ± 1275 ( 1153 - 4528)	1122 ± 606 ( 480 - 2048)	50 ± 16 ( 32 - 71)	27 ± 12 ( 13 - 47)

## 6.4 Discussion

This chapter presents an analysis of the cardiac and respiratory motion of the heart. X-ray angiography was used so that the normal physiologic motion patterns could be studied. Images could be acquired in a single shot with a temporal resolution of 33 ms. Breathing instructions were not given to the patients, so the images and measurements reflect normal tidal respiration. The effects of anxiety surrounding the invasive angiography procedure, which might be a source of physiologic changes in the patient's hemodynamic and respiratory condition, was not considered.

The displacement and velocity of the right coronary artery during a cardiac contraction was larger than for the left coronary tree. The RCA is found in the atrio-ventricular groove, located at the base of the heart. Studies of the mechanics of the heart have identified more motion at the base than at the apex. This topographic effect is consistent with the observation that among the left coronary vessels, the circumflex artery, which also follows the atrio-ventricular groove, has larger displacements and velocities. The displacement of the coronary arteries during the cardiac contraction was consistently directed towards the left, inferior, and anterior in all patients (Figures 6.2 and 6.3).

The diastolic rest period was found to be longer for the left coronary tree than for the right coronary artery (for a 3D motion limit of 1 mm,  $P=0.11$ , Student's t-test). This is consistent with higher mid-diastolic (diastasis) velocity measurements for the RCA (Tables 6.4 and 6.6).

Cardiac motion dominates the respiratory motion of the coronary arteries. Three dimensional displacements of up to 30 mm were observed in the proximal  $7.5 \pm 1.1$  cm of the right coronary artery. Tidal respiratory motion of the same anatomic region caused a maximum 3D displacement of 9.7 mm. In the proximal 5 cm of the left coronary tree – including the left main, left anterior descending, and left circumflex arteries – the maximum 3D displacement was 16.2 mm due to cardiac motion, and 9.3 mm due to breathing.

The displacement of the coronary arteries was directed caudally on inspiration. The motion in the left-right and anterior-posterior directions was more variable be-

tween patients. The direction of motion was nearly unbiased along these two axes, with the standard deviation of the motion larger than the mean value. Regional variation in respiratory displacement and velocity of the coronary arteries indicates that the motion is more complex than a simple 3D translation.

Differences in the inspiratory and expiratory maneuver duration led to larger mean respiratory velocity of the arteries during inspiration. The peak velocity during inspiration was higher than the peak velocity during expiration. Distal arterial segments demonstrated larger velocities than proximal segments.

The rest period at end-expiration was found to be very similar for the right coronary and left coronary studies. For an allowed 3D motion of 1 mm, the right coronary rest period was  $26\pm 8\%$  of the respiratory period, and  $27\pm 17\%$  for the left coronary artery. The end-inspiratory rest period was  $16\pm 8\%$  and  $11\pm 6\%$  for the right and left coronary arteries respectively.

### 6.4.1 Comparison with Previous Studies: Cardiac Motion

Measurements of coronary artery motion have been made previously. Most of the literature contains studies of the cardiac motion of the heart during a breath hold, with fewer reports of respiratory motion of the arteries. Confidence in our results is obtained by comparing them with reports of motion parameters found in the literature.

#### Displacement

A plot of RCA displacement as a function of the cardiac cycle found in [116] is very similar to Figure 6.2. Saranathan *et al.* acquired data using MRI with a voxel resolution of  $2.8\times 1.4\times 5$  mm, and peak RCA displacements of approximately 15-20 mm were reported. We found a range of 13-17 mm for peak RCA ostium 3D displacement.

Hofman *et al.* measured the in-plane cardiac motion of the coronary arteries in cross sectional images with a voxel sizes of  $1\times 1.4\times 5$  mm [117]. Measurements were reported for four landmarks which matched closely with the location of our

landmarks. They reported maximum in-plane displacements of  $25\pm 5$  mm for the RCA,  $9\pm 1$  mm for the LM,  $11\pm 4$  mm for the LAD, and  $12\pm 2$  mm for the LCx. Our 3D measurements were nearly identical:  $26\pm 3$  mm for  $RCA_O$ ,  $8\pm 2$  mm for  $LM_O$ ,  $10\pm 1$  mm for  $LAD_5$ , and  $12\pm 2$  mm for  $LCx_5$ . The close similarities in the 2D and 3D measurements suggests that the choice of imaging planes proposed in [118] may be effective because they minimize the effects of through-plane arterial motion during the cardiac cycle.

### Velocity

The 3D velocity of the coronary arteries during a cardiac contraction was measured with multi-slice spiral CT by Vembar *et al.* [20]. Systolic velocities of  $47\pm 22$  mm/s were reported at the RCA ostium, and  $91\pm 42$  mm/s at  $RCA_{AM}$ . Our data showed the same trend towards higher velocities at distal RCA landmarks, but we found higher velocities ( $RCA_0=70\pm 14$  mm/s;  $RCA_{AM}=102\pm 13$  mm/s).

For the left coronary tree, they reported systolic velocities of  $29\pm 12$  mm/s,  $24\pm 13$  mm/s, and  $68\pm 28$  mm/s, respectively, at the left main ostium, left anterior descending, and left circumflex arteries. In comparison, our measurements were  $35\pm 9$  mm/s,  $47\pm 9$  mm/s, and  $57\pm 10$  mm/s. The CT image reconstruction algorithm used by Vembar reconstructed images every 12.5% of the cardiac cycle by combining data acquired over a 250 ms window. The large degree of temporal averaging may explain the lower velocities they reported.

In another study, in-plane coronary artery motion velocity was measured using electron beam CT [119]. This technique provided a temporal resolution of 50 mm/s, but only 2D measurements of velocity. Reported peak systolic velocities of approximately 100 mm/s in the RCA, 75 mm/s in the left circumflex, and 30 mm/s in the LAD are more similar to our observations.

### Rest Period

Wang *et al.* studied the rest period during the cardiac contraction with x-ray angiograms acquired during a breath hold [120]. The mid-diastolic rest period was

defined as motion less than 1 mm in any of the orthogonal directions visualized in two orthogonal projection images. The upper bound on the 3D motion is thus  $\sqrt{3}=1.73$  mm, however depth dependent amplification of objects in projection images was not corrected. The mean rest period durations that were reported were 120 ms (range, 66-200 ms) for the right coronary artery and 161 ms (range, 66-333 ms) for the left coronary tree. For a 3D motion cutoff of 1.75 mm, we measured similar mean rest period durations of 124 ms (range, 35-222 ms) for the right coronary artery and 178 ms (range, 94-257 ms) for the left coronary tree.

#### **6.4.2 Comparison with Previous Studies: Respiratory Motion**

Biplane x-ray coronary angiography provides higher temporal and spatial resolution images than MR, and the x-ray images can be used to make 3D measurements. Yet, x-ray angiography has not been used to study respiratory motion because of the difficulty in separating the cardiac and respiratory motions of the arteries. This is now possible using the method described in Chapter 5.

The few published experimental reports on the motion of the coronary arteries due to breathing use ECG-gated MR imaging to freeze the effects of cardiac motion. The nature of the MR acquisition has resulted in two general classes of imaging protocols: (1) 2D and 3D imaging at multiple breath holds simulating normal breathing; and (2) 2D real time imaging during free breathing. Neither of these methods is suited for measuring 3D respiratory motion during free breathing.

A discussion of the respiratory displacements reported in the literature follows. To the best of our knowledge there are no reports of coronary velocity and rest period duration due to respiratory motion.

##### **Displacement**

Wang *et al.* measured the tidal respiratory displacement of the coronary arteries in ten healthy volunteers using 2D MR imaging with a voxel size of  $1.1 \times 2.2 \times 5$  mm [61]. In ten patients the displacement of the RCA ostium was  $10.5 \pm 4.8$  mm in the cranio-

caudal direction and  $2.3 \pm 1.4$  mm in the anterior-posterior direction. The LAD was reported to move  $13.1 \pm 4.1$  mm and  $2.0 \pm 0.7$  mm in those axes. The cranio-caudal displacements are nearly three times larger than we measured ( $RCA_0$ :  $4.1 \pm 1.6$  mm;  $LAD_5$ :  $4.7 \pm 1.8$  mm).

These large differences may be an artifact of the imaging method used by Wang. Since images were acquired during a breath hold, the tidal respiratory range was sampled by asking the patients to hold their breath at different respiratory positions. The average diaphragmatic displacement was reported to be 20 mm, which is larger than measurements made during free breathing. This information suggests that the simulated tidal breathing range was in fact larger than the range of motion that would be found during spontaneous tidal breathing. Results supporting this hypothesis were presented in [121].

Secondly, displacement measurements were made in 2D images, which raises the concern that the measurements made between two images at different respiratory positions did not track material points. Finally, compared to the 33 ms temporal resolution we obtained with x-ray angiography, the temporal resolution of the MR acquisition was 117 ms, and images were created by combining data collected across 16 heart beats. Based on the results from Section 6.2.3, this temporal window could be associated with up to 1.75 mm of motion in the right coronary artery, and 1 mm in the left coronary. Temporal averaging may have led to displacement caused by the cardiac contraction, or variances in beat-to-beat motion of the arteries, to be classified as respiratory motion.

McLeish *et al.* reported the respiratory displacement of a point along the RCA using 3D MRI with 25-30 second breath holds [63]. The temporal resolution of the images was 180 ms, and the spatial resolution was  $1.4 \times 1.4 \times 6$  mm. The mean displacement was  $8.2 \pm 3.4$  mm in 9 patients, and  $17 \pm 4.3$  mm in 8 volunteers. A Student's t-test indicates a statistically significant difference between the two populations with  $P < 0.0003$ . It is difficult to directly compare the results since the position of their RCA landmark is not known, but their patient results are similar to the 3D displacements we observed at  $RCA_{(0.5)AM}$  ( $6.4 \pm 1.9$  mm) and  $RCA_{AM}$  ( $7.2 \pm 2.2$  mm).

LM cranio-caudal displacements of  $9 \pm 3$  mm during tidal respiration was reported

by Danias *et al.* using real-time MR imaging in twelve healthy volunteers [62]. Two dimensional slices with a voxel size of  $(0.75-2.2) \times (0.75-2.2) \times 4$  mm were acquired during one  $100 \pm 10$  ms temporal window. These free breathing results are smaller than those reported by Wang, but still larger than our measurements.

### 6.4.3 Implications for MR Coronary Imaging

Magnetic resonance imaging has the potential to be an important non-invasive imaging method for detection and staging of coronary artery disease. The coronary arteries have diameters ranging from 2.0-3.9 mm for the proximal-to-distal right coronary artery, and 1.8-3.7 mm for the left main, and proximal-to-middle segments of the left anterior descending and left circumflex arteries [122]. Detection of a 25% stenosis of the 1.8 mm diameter vessel requires an image resolution of approximately 0.5 mm.

Coronary artery motion complicates magnetic resonance coronary imaging. In general, motion during an MR acquisition causes blurring and ghosting artifacts in the images [37, 38]. Even though cardiac motion of the arteries is larger than their respiratory motion, coronary MR imaging is plagued by the later. One hypothesis is that the beat-to-beat variability in cardiac motion is smaller than breath-to-breath variability in respiratory motion [120].

Two dimensional MR coronary images can be acquired during a breath hold [26, 27]. These ECG gated acquisitions with short signal readouts have essentially frozen the motion of the heart during the cardiac contraction. However, 2D imaging requires the use of thick imaging slices (3–5 mm) which can cause partial volume effects and signal averaging when visualizing sub-millimeter pathologies. Measurements of lumen area and wall thickness could be distorted by oblique sectioning of the artery.

Misregistration of multiple slices caused by breath-hold inconsistency makes visualization of tortuous and non-planar vessels difficult with 2D imaging [25]. Three dimensional (3D) MRCA can provide higher resolution, higher SNR, isotropic volumetric images. However, these methods require longer imaging times, and introduce the problem of respiratory motion. Respiratory blur in 3D coronary imaging can lead

to overestimation of vessel lumen size and undetected stenoses [123].

Gating the MR acquisition to some phase of the cardiac and respiratory cycles is one method for freezing the motion of the coronary arteries. The rest period durations measured in this chapter can be used to set bounds on the temporal width of the imaging window. Increasing the amount of physiologic motion that would be acceptable during imaging, would increase the duration during which data could be acquired. This would shorten the total imaging time, but introduce more blurring in the images. On the other hand, decreasing the size of the imaging window might reduce the potential for motion artifacts, but it will increase the total scan duration.

### Scan Efficiency

Scan efficiency is defined as the amount of time during which data is acquired divided by the elapsed time of the scan. Using the average heart rate (64 beats per minute) and respiratory rate (15 breaths per minute) of the patients we studied, we can calculate a sample scan efficiency. Suppose that a 3D volume with half millimeter isotropic resolution is desired, and a signal readout (TR) can be acquired in 5 ms. A 6 cm thick 3D slab would require 120 phase encoding steps in the Z direction, multiplied by 256 phase encodes in Y.

Allowing 0.5 mm cardiac motion corresponds to a temporal imaging window of 55 ms during diastasis of the cardiac cycle, so that 11 phase encoding steps could be acquired each heartbeat. Similarly, if we allow 0.5 mm of respiratory motion, then the potential imaging window would be 17% of the respiratory cycle at end-expiration. However, data can only be acquired when diastasis and end-expiration coincide. Running the following simple simulation:

```

1  HeartRate          = 64
2  Respiratory Rate = 15
3
4  Cardiac_Period      = 60/HeartRate      * 1000      %% (msec)
5  Respiratory_Period = 60/RespiratoryRate * 1000      %% (msec)
6
7  Cardiac_ImagingWindow = 55              %% (msec)
```

```

8   Respiratory_ImagingWindow = (.17)*Respiratory_Period    %% (msec)
9
10  PhaseEncodes = 0
11  Time = 0
12
13  while PhaseEncodes < (120 * 256)
14
15      Time = Time + 1
16
17      if ( mod(Time, Respiratory_Period) < Respiratory_ImagingWindow)
18          and
19              ( mod(Time, Cardiac_Period ) < Cardiac_ImagingWindow)
20          then
21              PhaseEncodes = PhaseEncodes + 1
22          endif
23
24  endwhile

```

reveals that acquiring the necessary data would take approximately 51 minutes. The scan efficiency would be  $(120 \times 256 \times 5 \text{ milliseconds}) / 51 \text{ minutes} = 5.4\%$ .

Heart rate and respiratory rate variability can be introduced by adding the following statements at line 23:

```

23.1 // Allow a 5% beat-to-beat change in R-R interval
23.2   if new heart beat
23.3       Cardiac_Period = (60/HeartRate*1000) +/- 5%
23.4   endif
23.5
23.6 // Allow a 10% breath-to-breath change in respiratory period
23.7   if new breath
23.8       Respiratory_Period = (60/RespiratoryRate*1000) +/- 10%
23.9       Respiratory_ImagingWindow = (.17)*Respiratory_Period
23.10  endif

```

The cardiac period was modeled as a normal distribution with  $\mu=64$  beats per minute and  $\sigma = 64 \times (5\%)$ . The respiratory period was modeled as a normal distribution with  $\mu=15$  breaths per minute and  $\sigma = 15 \times (10\%)$ . The simulation was performed 10 times,

and the mean scan time was  $51 \pm 1$  minutes. Variations in the heart and breathing rate did not significantly change the scan efficiency.

Scan durations of this length are not clinically practical. In addition, longer scans would increase the chance that normal physiologic variability would prevent the heart from ever returning to the reference state which existed at the start of the image acquisition.

Motion correction is one approach for increasing scan efficiency. One popular method works by translating the imaging slab by an amount proportional to the diaphragmatic displacement, which is monitored in real time during the scan. The proportionality constant has been an active topic of research [61, 62, 30, 53, 121, 105, 63, 124]. Scan efficiency is thus increased by compensating for respiratory motion, and acquiring data during more of the respiratory cycle.

Our measurements show spatial variations in displacement and velocity of the coronary arteries during breathing, which indicates that the true motion of the arteries during breathing is more complex than a translation. In Chapter 2, we showed that motion and deformations which can be classified as affine transformations are correctable during MR imaging [65, 66]. Patient specific correction factors could be computed at scan time, and used to correct the image acquisition [67].

The measurements of respiratory motion and deformation of the coronary arteries presented in this chapter can be analyzed further in the context of MR motion correction. One can ask whether the motion can be explained using translations alone, or whether more complex models are needed.

Three different motion models were studied: (1) a 3D translation; (2) a 3D rigid body transformation; and (3) a 3D affine deformation. The position of the coronary tree at end-expiration served as the reference state, and the coronary trees at the other respiratory phases were registered to it. The rest period duration was then computed using the same method described in Section 6.1.3. We refer to this new metric as the motion corrected rest period (MCRP).

Figure 6.18 shows the effect of motion correction on the rest period at end-expiration. The graph shows that as the degrees of freedom of the motion model are increased (translation < rigid < affine), the MCRP duration also increases. For

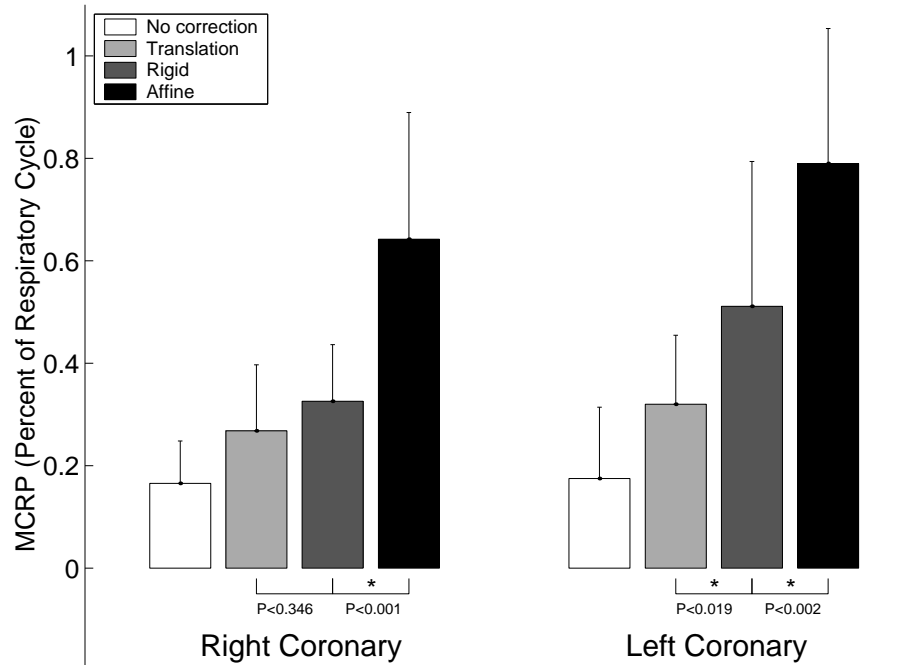


Figure 6.18: Motion corrected rest period (MCRP) duration for the respiratory cycle at end-expiration: A comparison of three different motion models. The physiologic motion is shown as a baseline reference. Two Bonferroni corrected t-tests were performed for each artery to test for incremental differences in the MCRP. A group-wise statistical significance of  $\alpha < 0.05$  is indicated by a star (\*). P-values are provided for all t-tests.

a tolerated 3D motion of 0.5 mm, the physiologic rest period of the left coronary tree was measured as  $18 \pm 14\%$  of the tidal respiratory cycle.

Translation was able to model the motion of the arteries for  $32 \pm 13\%$  of the tidal respiratory cycle for the same motion tolerance. The MCRP increased to  $51 \pm 28\%$  of the cycle with the addition of rotational degrees of freedom in the rigid body motion model. The affine motion model extended the MCRP to  $79 \pm 26\%$  of the respiratory cycle.

The rigid body motion model modeled the respiratory motion for a significantly longer portion of the respiratory cycle than translation motion alone ( $P < 0.019$ , Bonferroni t-test for paired samples and two comparisons [115]). The affine deformation model modeled the respiratory motion for a significantly longer fraction of the respiratory cycle than the rigid body transformation ( $P < 0.002$ , Bonferroni t-test for paired

samples and two comparisons).

The longer rest periods that could be achieved with the different motion correction techniques could translate into shorter imaging times. Performing the scan efficiency simulation again with the motion corrected rest periods yields scan efficiencies of 9.5%, 15.0% and 23.3% respectively, for the translation, rigid body, and affine motion correction techniques. Affine motion correction could reduce the 51 minute scan to a more manageable 12 minutes.

For the right coronary artery, there was no statistical improvement with the rigid body model (MCRP mean,  $33\pm 11\%$ ) over the translation motion model (MCRP mean,  $27\pm 13\%$ ). The affine motion model was able to capture the motion over  $64\pm 25\%$  of the respiratory cycle. This was a statistically significant improvement over the rigid body motion model ( $P < 0.001$ , Bonferroni t-test for paired samples and two comparisons).

Figure 6.19 shows the utility of the different motion models for different imaging conditions. Consider an application where the image resolution requirement is more relaxed. If 1.5 mm of motion could be tolerated during the acquisition, than the graph shows that the largest improvement in scan efficiency for the left coronary tree would be obtained by using a translation motion correction method. The rigid body correction technique would not reduce scan time significantly. The affine motion correction technique would improve scan efficiency, but the amount of time saved might not warrant the use of the more complicated affine correction method in lieu of the simpler translation correction.

### **Navigator echos**

MR motion correction depends on having a way to detect the respiratory state so that the appropriate correction parameters can be applied to prospectively or retrospectively correct the acquisition. Navigator echos can be interleaved with the image acquisition in order to quantify the motion of the diaphragm, the heart, and/or the chest wall [28, 52, 56, 66]. These measurements could be used to estimate the motion parameters – translation, rigid body, or affine – of the heart using *a priori*

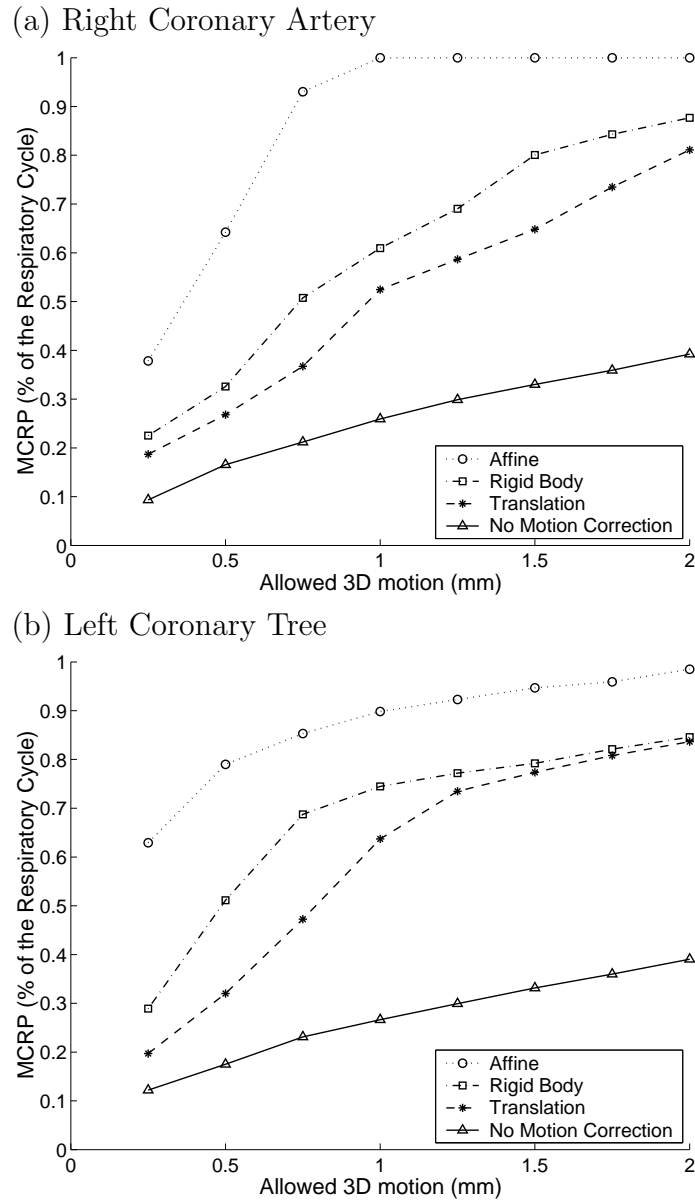


Figure 6.19: Respiratory rest period duration for different imaging requirements: A comparison of three different motion models. MCRP: motion corrected rest period duration in percent of the respiratory cycle. This is a temporal analog of Figure 6.20.

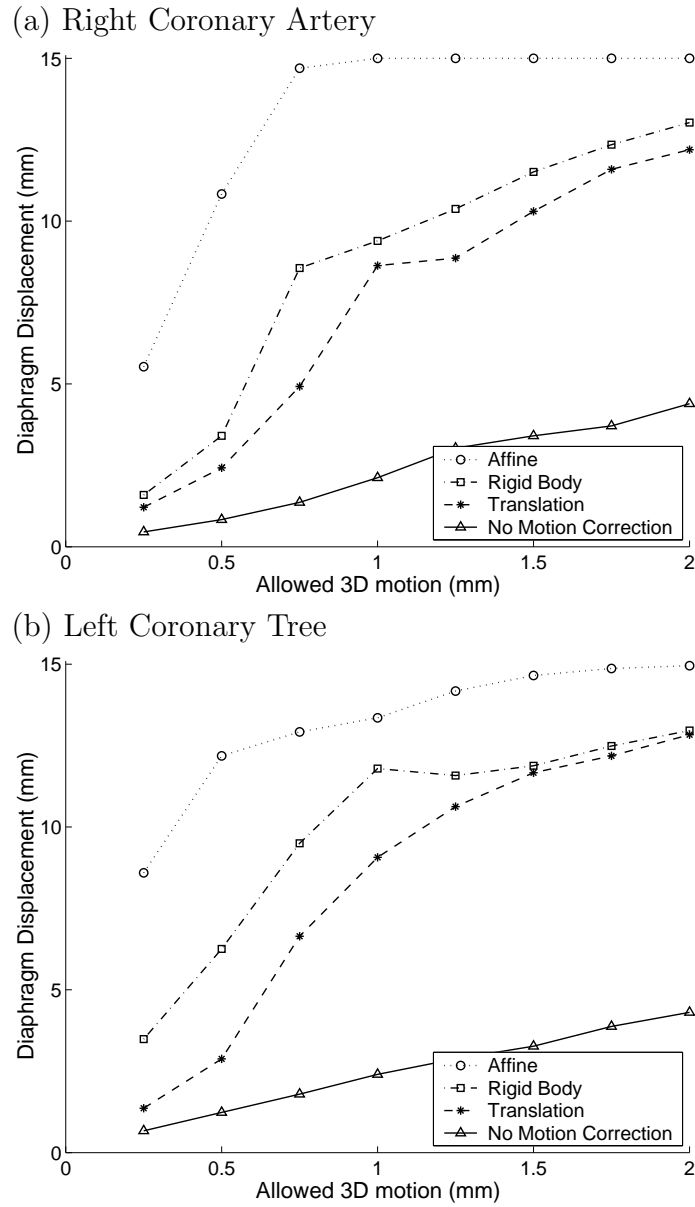


Figure 6.20: Respiratory rest period duration for different imaging requirements: A comparison of three different motion models. Diaphragmatic displacement was not directly measured, but estimated for each patient using the respiratory phase and an average respiratory displacement of 15 mm. This is a spatial analog of Figure 6.19.

knowledge learned from this and other studies of the heart's motion.

In this study, we did not acquire any true one dimensional measurements which are analogous to MR navigator signals. Nonetheless, respiratory phase was based on intra-patient normalized diaphragmatic displacement as seen in the x-ray angiograms. Based on previous reports [60, 62, 53, 121, 124], we use 15 mm as the maximum tidal displacement of the diaphragmatic dome, and map each patient's displacement to the interval [0,15] mm. This transformation allows the rest period calculations to be converted from the temporal domain into a spatial domain reflective of the diaphragmatic displacement. Figure 6.20 is a spatial equivalent of Figure 6.19.

## 6.5 Conclusion

The cardiac and respiratory motion of the coronary arteries was measured in ten patients from free breathing x-ray angiograms. Coronary motion due to the cardiac contraction is 2-4 times larger than the respiratory motion during tidal breathing in the supine human. For the proximal-to-middle segments of the right coronary artery, a cardiac rest period ( $\leq 1$  mm total 3D displacement) was found to last  $76 \pm 34$  ms at end-systole and  $64 \pm 41.6$  ms in mid-diastole (diastasis). The rest period was found to be  $80 \pm 25$  ms at end-systole and  $112 \pm 42$  ms at mid-diastole for the proximal 5 cm of the left coronary tree.

The respiratory rest period was found to be longest at end-expiration. The mean rest period duration (in percent of the respiratory period) was  $26 \pm 8\%$  for the right coronary artery, and  $27 \pm 17\%$  for the left coronary tree. Three dimensional translation motion correction of respiratory motion during magnetic resonance imaging of the left coronary tree could improve scan efficiency by a factor of two over non-motion corrected techniques. Rigid-body and affine motion correction provide three-fold and four-fold increases in efficiency, respectively. For the right coronary artery, the rigid body method was just as effective as translational motion correction for improving scan efficiency (two-fold increase). Affine motion correction increased efficiency by approximately three-to-four fold. The variability of respiratory motion demands an adaptive patient-specific paradigm for MR coronary imaging.